European Journal of Medicinal Chemistry 299 (2025) 118068

Contents lists available at ScienceDirect

European Journal of Medicinal Chemistry

journal homepage: www.elsevier.com/locate/ejmech

Research paper

Vitamin K-Trolox synergism realized in hybrid neuroprotectant with potent anti-ferroptosi/oxytosis activity, reduced toxicity, and *in vivo* efficacy in Alzheimer's disease mouse model

Feng He [a,b,1], Julian Hofmann [b,1], Eleonora Poeta [c], Barbara Monti [c,e], Lucie Crouzier [d], Tangui Maurice [d], Michael Decker [b,*]

[a] State Key Laboratory of Eye Health, Eye Hospital, Wenzhou Medical University, Wenzhou, 325027, China
[b] Julius-Maximilians-Universität Würzburg (JMU), Institut für Pharmazie und Lebensmittelchemie, Pharmazeutische und Medizinische Chemie, Am Hubland, 97074, Würzburg, Germany
[c] Department of Pharmacy and Biotechnology, University of Bologna, Via Selmi 3, 40126, Bologna, Italy
[d] MMDN, Univ Montpellier, EPHE, INSERM, Montpellier, France
[e] IRCCS Istituto delle Scienze Neurologiche di Bologna, 40139 Bologna, Italy

ARTICLE INFO

Keywords:
Vitamin K
Trolox
Oxytosis
Ferroptosis
Alzheimer's disease

ABSTRACT

In pursuit of developing advanced neuroprotective agents for neurodegenerative disorders, we rationally designed a series of novel hybrid molecules through structural integration of a vitamin K derivative with well-known antioxidants (ferulic acid, melatonin, α-lipoic acid, and Trolox, respectively). Systematic pharmacological evaluation revealed that most hybrids exhibited superior antioxidant activity in both DPPH radical scavenging and ORAC assays. Among these, a Trolox-vitamin K conjugate (compound **16e**) emerged as a promising compound, demonstrating exceptional neuroprotective efficacy across multiple neuronal injury models, including oxytosis, ferroptosis, and ATP depletion in HT22 hippocampal neurons. Mechanistic studies confirmed that this compound preserved synergistic cytoprotective effects of its parent pharmacophores against ferroptosis while concurrently exhibiting immunomodulatory activity in microglial cells. Notably, it significantly ameliorated Aβ_{25-35}-induced cognitive deficits in a murine Alzheimer's disease model at a very low dose (0.1 mg/kg, i.p.), outperforming conventional neuroprotectants in therapeutic potency. These findings position this Trolox/vitamin K hybrid molecule as a neuroprotective candidate with translational potential for treating neurodegenerative pathologies.

1. Introduction

Neurodegenerative disorders are characterized by multifactorial etiopathogenesis encompassing pathological protein aggregation, chronic neuroinflammation, redox imbalance, and programmed neuronal death pathways [1,2]. Alzheimer's disease (AD), the most prevalent neurodegenerative condition, has been historically dominated by the amyloid cascade hypothesis positing β-amyloid (Aβ) aggregation as its primary driver. However, the staggering 99.6 % failure rate of Aβ-targeted therapies in 2002–2012 clinical trials has necessitated a paradigm shift toward alternative pathological mechanisms, particularly oxidative stress-mediated neurodegeneration and glial-mediated inflammatory cascades [3].

Emerging evidence implicates oxytosis/ferroptosis, an iron-dependent lipid peroxidation cascade, as a critical oxidative cell death modality in AD pathogenesis. [2,4]. The Maher lab pioneered oxytosis-pathway-driven drug discovery, identifying curcumin-derived clinical candidate J147 (**1**) and fisetin analog CMS121 (**2**), both currently advancing through AD therapeutic pipelines [5]. The Stockwell lab firstly described the ferroptosis pathway and identified compound ferrostatin-1 (**3**) as a potent ferroptosis inhibitor (EC_{50} = 60 nM) with demonstrated neuroprotective efficacy [6]. The development of novel neuroprotectants can not only yield drug candidates for the treatment of neurodegenerative diseases, but also can provide molecular tools to uncover new aging and disease pathways. Our laboratory has leveraged oxytosis/ferroptosis phenotype screening and privileged

* Corresponding author.
E-mail address: michael.decker@uni-wuerzburg.de (M. Decker).
[1] These authors contributed equally to this work.

https://doi.org/10.1016/j.ejmech.2025.118068
Received 30 June 2025; Received in revised form 7 August 2025; Accepted 14 August 2025
Available online 16 August 2025

pharmacophore hybridization to identify multifunctional neuroprotectants. Rational modification of flavonoid cores (**4**, **5**) [7–9], tetrahydroisoquinazoline motifs (**6**) [10,11], cannabinoid receptor 2 (CB2)-targeting scaffolds (**7**) [12], and curcumin azobioisosteres (**8**) [13] has yielded compounds with high, even *in vivo* neuroprotective efficacy.

The Chou group systematically explored the structure-activity relationships (SAR) of vitamin K derivatives, identifying menaquinone-based analogs **9** and **10** with enhanced neuroprotective profiles against oxytosis (Fig. 1) [14]. Parallelly, Segal and colleagues developed naphthoquinone-tryptophan hybrids exhibiting dual inhibition of amyloid-β aggregation and tau-derived PHF6 fibrillization, highlighting their translational potential for AD therapeutics [15,16]. Of note, vitamin K analogs confer ferroptosis resistance through a non-canonical pathway involving ferroptosis suppressor protein 1 (FSP1), operating independently of the glutathione peroxidase-4 (GPX4) axis [17].

Molecular hybridization represents a valuable strategy for enhancing pharmacological activities and optimizing drug candidates targeting complex diseases such as neurodegenerative disorders. Notably, Trolox-tacrine hybrids demonstrated reduced *in vivo* toxicity [18]. Ferulic acid and melatonin hybrids with histone deacetylase (HDAC) or butyrylcholinesterase (BChE) inhibitors showed enhanced neuroprotection in Alzheimer's disease models [19,20]. Lipoic acid-Adenosine A_2A receptor antagonist hybrids exhibited significant efficacy in neuropathic pain models [21]. Capitalizing on these insights, we rationally designed a novel class of hybrid neuroprotectants through strategic molecular hybridization. Our approach integrates the optimized vitamin K scaffold (**10**) with privileged antioxidant pharmacophores to engineer multifunctional agents targeting complementary neuroprotective pathways. Herein, we report the synthesis and comprehensive pharmacological evaluation of this hybrid series with particular emphasis on their synergistic antioxidant capacity and multimodal neuroprotective efficacy (Fig. 2).

2. Results and discussion

2.1. Chemistry

As shown in Scheme 1, synthesis of compound **6** started from 1,4-naphthoquinone (**11**). Reagent **11** could undergo Michael addition reaction with 4-(aminomethyl)aniline to afford intermediate **12** at ambient conditions. Ferulic acid was activated by ethyl chloroformate and coupled with intermediate **12** to afford intermediate **13**, which was subsequently hydrolyzed under basic solution to produce compound **14**. Compounds **16a-e** were synthesized from corresponding acids as described in Scheme 2. Briefly, carboxylic acids (ferulic acid, cinnamic acid, lipoic acid, and Trolox) were activated by HBTU and reacted with ethylenediamine or butane-1,4-diamine to produce corresponding intermediates **15a-e**. Without further purification, intermediates **15a-e** were reacted with 1,4-naphthoquinone in ethanol through Michael addition reaction to synthesize compounds **16a-e**.

Owing to the inherent reactivity of its catechol moiety, caffeic acid-derived hybrid **21** required a protective group strategy (Scheme 3). Initial acetylation of caffeic acid with acetic anhydride in pyridine provided intermediate **17**. Activation of compound **17** with ethyl chloroformate and coupling with *N*-Boc-ethylenediamine yielded protected intermediate **18**. Boc deprotection of **18** with TFA/DCM (1:10), followed by *in situ* Michael addition with 1,4-naphthoquinone, afforded quinone adduct **20**. Then the deacetylation of intermediate **20** and compound **21** was achieved with an overall yield of 15 %.

The synthesis of compounds **22**, **24**, and **25** is described in Scheme 4. Compounds **22** and **24** were obtained from 5-methoxyltryptamine by reacting with 1,4-naphthoquinone (**11**) and 2,3-dimethoxycyclohexa-2,5-diene-1,4-dione (**23**), respectively. Compound **25** was obtained by Michael addition from 2,3-dimethoxycyclohexa-2,5-diene-1,4-dione and reagent **23**.

2.2. Preliminary screening

The neuroprotective potential against oxytosis, an oxidative stress-induced cell death pathway, was evaluated in murine hippocampal

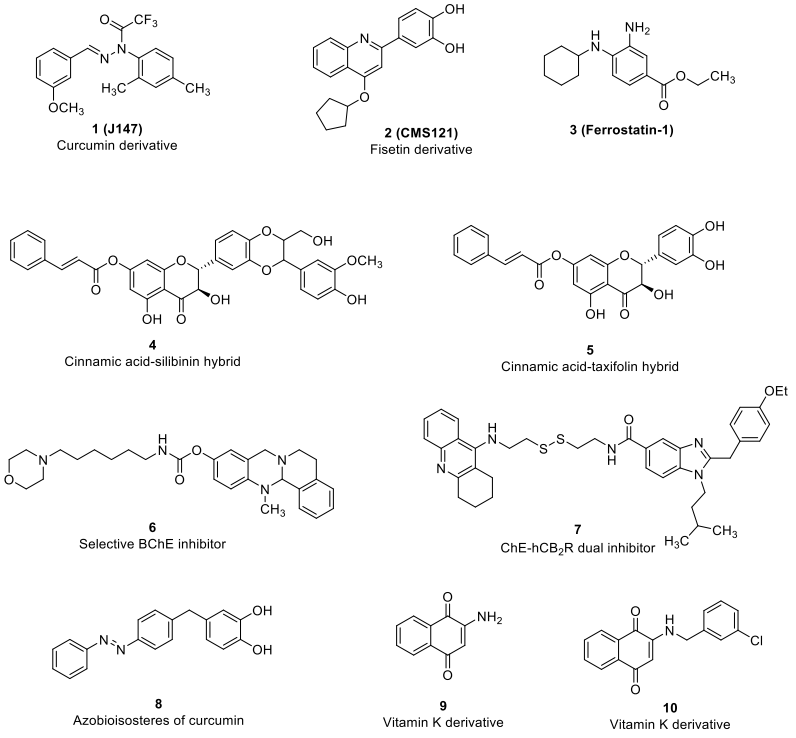

Fig. 1. A selection of neuroprotectants based on the oxytosis/ferroptosis pathway.

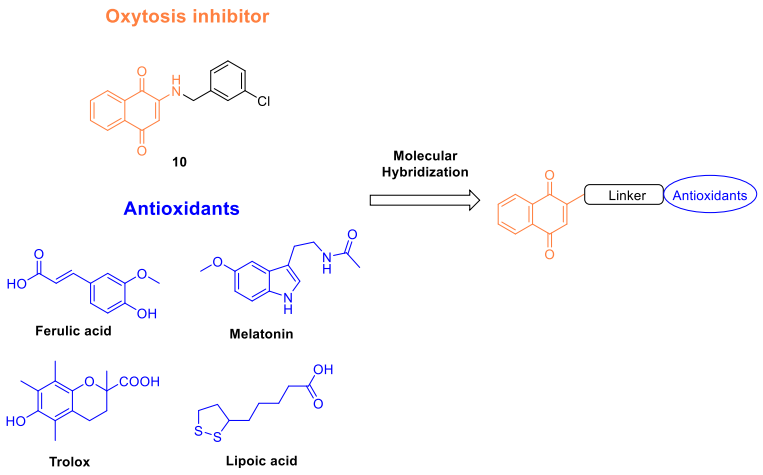

Fig. 2. Design of hybrid neuroprotectants based on vitamin K derivatives.

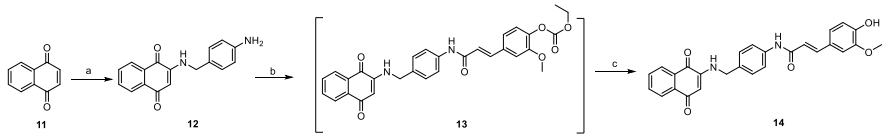

Scheme 1. Synthesis of Compound 14 from 1,4-Naphthoquinone (3)[a]. [a]Reagents and conditions: (a) 4-(aminomethyl)aniline, EtOH, r.t. 40 %; (b) ferulic acid, ethyl chloroformate, TEA, THF, 0 °C to r.t.; (c) KOH, MeOH, r.t., 15 %.

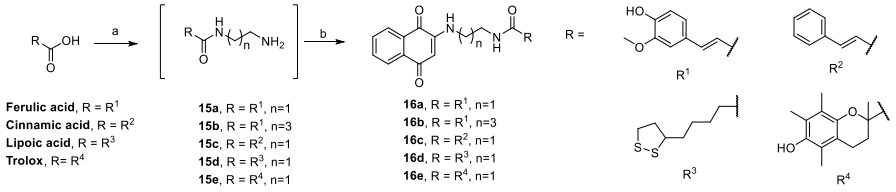

Scheme 2. Synthesis of Compounds 16a-e from Corresponding Acids[a]. [a]Reagents and conditions: (a) ethylenediamine for **15a** and **15c-e**, butane-1,4-diamine for **15b**, HBTU, TEA, DCM, r.t.; (b) 1,4-naphthoquinone, EtOH, r.t., 1 %–48 %.

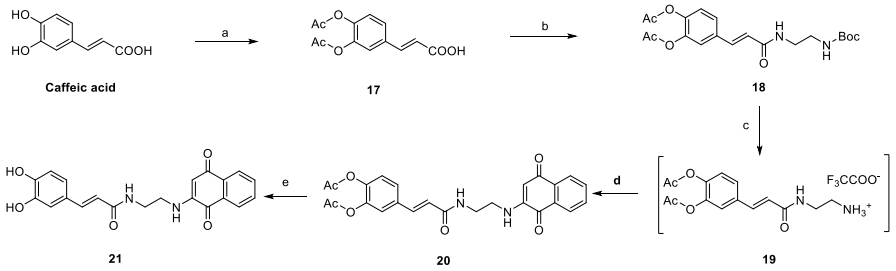

Scheme 3. Synthesis of Compound 21 from Caffeic Acid[a]. [a]Reagents and conditions: (a) Ac_2O, pyridine, r.t., 83 %; (b) i) ethylenediamine, Boc_2O, TFA, MeOH, 0 °C to r.t.; ii) ethyl chloroformate, TEA, THF, 0 °C to r.t., 88 %; (c) TFA, DCM, r.t.; (d) 1,4-naphthoquinone, TEA, EtOH, r.t., 79 %; (e) KOH, MeOH, r.t., 26 %.

HT22 cells subjected to glutamate challenge (see Fig. 3). Compound **10**, demonstrating significant neuroprotective efficacy at 10 μM, was selected as the parent scaffold for molecular hybridization. To leverage potential synergistic effects, compound **14** was designed by hybridizing compound **10** with a ferulic acid pharmacophore via a benzyl linker. While compound **14** exhibited no significant activity at concentrations of 5 or 10 μM, the aliphatic linker proved critical for activity restoration. Specifically, derivative **16b**, incorporating a four-carbon spacer, conferred significant neuroprotection at 10 μM. Notably, the optimal activity profile was achieved with the two-carbon-linked analogue **16a**, which demonstrated potent neuroprotective effects at both 5 and 10 μM.

Subsequently, retaining the optimal two-carbon linker, compound **16c** conjugated with cinnamic acid, and compound **21** conjugated with caffeic acid, respectively, were investigated to evaluate the significance of phenolic acid substituents. Compound **16c** lacked neuroprotective efficacy at both 5 and 10 μM, while compound **21** was inactive at 5 μM, which indicates that the ferulic acid moiety confers superior enhancement of neuroprotective activity against glutamate-induced insult compared to cinnamic acid or caffeic acid. Further exploration involved replacing ferulic acid with established antioxidants, including melatonin, Trolox, and lipoic acid. Among these analogs, the Trolox conjugate **16e** and melatonin conjugate **22** exhibited neuroprotective activity comparable to compound **16a** at both 5 μM and 10 μM. Despite structural similarity conferred by its quinone moiety, ubiquinone-derived

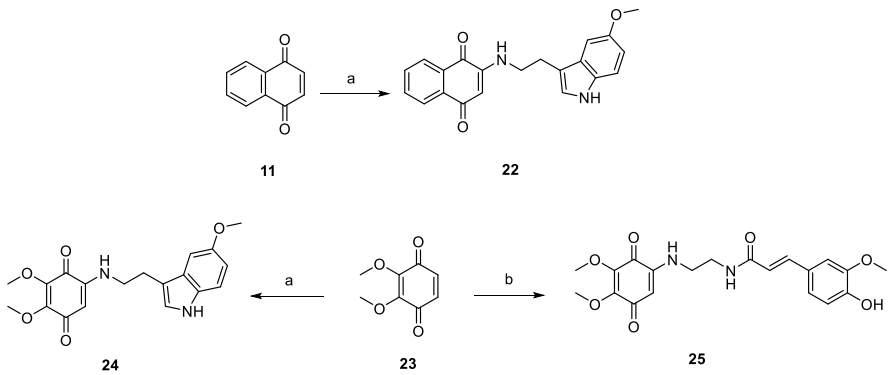

Scheme 4. Synthesis of Compounds 22, 24, and 25 from 1,4-Naphthoquinone and 2,3-Dimethoxycyclohexa-2,5-diene-1,4-dione[a]. [a]Reagents and conditions: (a) 5-methoxytryptamine, EtOH, r.t., 5 %–8 %; (b) i) ferulic acid, ethylenediamine, HBTU, TEA, DCM, r.t.; ii) EtOH, r.t., 6 %.

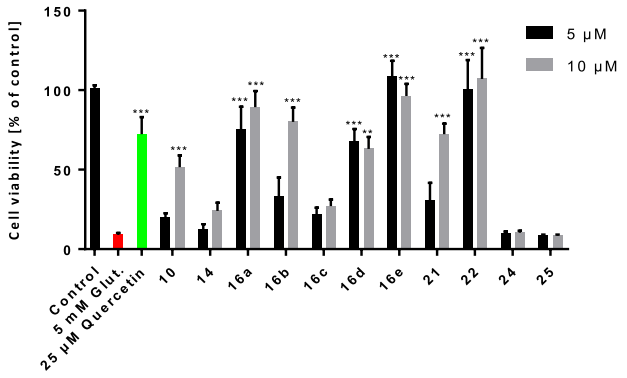

Fig. 3. Neuroprotection of hybrid vitamin K derivatives at 5 and 10 µM, respectively, against glutamate induced oxytosis in HT22 cells. Quercetin (at 25 µM) served as a positive control (green) while 5 mM glutamate was used to induce toxicity (red). Data is presented as means ± SEM of three independent experiments and results refer to untreated control cells (black). Statistical analysis was rendered using One-way ANOVA followed by Dunnett's multiple comparison posttest referring to cells treated with 5 mM glutamate. Levels of significance: $^{**}p < 0.01$, $^{***}p < 0.001$. (For interpretation of the references to colour in this figure legend, the reader is referred to the Web version of this article.)

hybrids **24** and **25** failed to protect HT22 cells from oxytosis, indicating specificity beyond the quinone pharmacophore. Collectively, based on their superior neuroprotective potency relative to the initial lead compound **10**, hybrids **16a**, **16e**, and **22** were prioritized for further investigation.

2.3. Physicochemical antioxidant parameters

All hybrid compounds were designed to retain the intrinsic antioxidant properties of their parent compounds. Antioxidant activity was evaluated using the 2,2-diphenyl-1-picrylhydrazyl (DPPH) radical scavenging assay, which measures electron transfer (ET)-based reducing capacity, and the oxygen radical absorbance capacity (ORAC) assay, which quantifies hydrogen atom transfer (HAT)-based peroxyl radical quenching.

In the DPPH assay, four ferulic acid hybrids (**14**, **16a**, **16b**, **25**) exhibited potent and comparable radical scavenging activity (EC_{50} = 29.0, 26.1, 27.2, and 28.4 µM, respectively), albeit less potent than unmodified ferulic acid (EC_{50} = 19.7 µM) (Table 1). Neither the linker moieties nor the quinone pharmacophores contributed significantly to DPPH reduction, consistent with the inactivity of reference compounds **9** and **10** [14]. In contrast, compounds **16e** and **21** demonstrated superior scavenging capacity (EC_{50} = 15.4 and 9.0 µM, respectively), comparable to their parent antioxidants Trolox and caffeic acid. As anticipated, melatonin, lipoic acid, cinnamic acid derivatives, and all ubiquinone hybrids lacked DPPH scavenging activity, consistent with the absence of phenolic groups essential for ET-based mechanisms.

In the ORAC assay, most target compounds displayed significant peroxyl radical scavenging activity, with ORAC values ranging from 1.6 (**16e**) to 3.6 (**21** and **25**) Trolox equivalents. Notably, peroxyl radicals (ORAC = 1.5), exhibiting activity comparable to compounds **16e** and **22**. Compounds **21** and **25** exhibited the highest ORAC values (3.5), despite demonstrating limited neuroprotection at 5 µM in the oxytosis assay. ORAC values for compounds **10**, **16c**, and **16d, respectively,** could not be determined due to intrinsic fluorescence interference.

In summary, compounds **16a**, **16e**, and **22** demonstrated promising neuroprotective activity in the oxytosis assay. They also exhibited potent antioxidant capacity both DPPH and ORAC assays except compound **22** (only active in ORAC assay). Compound **10** displayed a radical scavenging profile analogous to melatonin. No significant correlation was observed between neuroprotective efficacy and antioxidant capacity measured by DPPH or ORAC. This disconnection, consistent with prior studies [7,11], may arise from differences in cellular permeability, target engagement, or the contribution of non-radical scavenging mechanisms to neuroprotection. Although elevated lipophilicity (higher calculated Log P for **16a**, **16e**, **22**) may facilitate cellular access, it is, of course, not the sole determinant of neuroprotection. This is evidenced by the inactive, more lipophilic analogue **14**, precluding a direct Log P-efficacy correlation within this series. Moreover, with the exception of caffeic acid-based compound **21** and two ubiquinone-derived hybrids (compounds **24** and **25**), respectively, all other hybrid compounds exhibit a high probability of crossing the blood-brain barrier (BBB), as indicated by predictions from Deep-PK, suggesting their potential therapeutic application in neurodegenerative diseases.

2.4. Neuroprotection against oxytosis, ferroptosis and ATP depletion

Encouraged by the potent neuroprotective effects and pronounced antioxidant capacities exhibited by compounds **16a**, **16e** and **22**, we further evaluated these compounds at lower concentrations in oxytosis (Fig. 4A–D, G, J), ferroptosis (Fig. 4B–E, H, K), and ATP depletion assays (Fig. 4C–F, I, L) to more comprehensively characterize their neuroprotective profiles.

In the oxytosis assay, compounds **16a** (Fig. 4D) and **13** (Fig. 4J) demonstrated neuroprotective activity comparable to compound **10** (Fig. 4A), with all three compounds losing efficacy at concentrations ≤1.56 µM. Notably, compound **16e** maintained significant protection at both 1.56 and 0.75 µM (Fig. 4G), establishing it as the most potent hybrid compound in this paradigm.

RSL3 is a classical ferroptosis inducer that elevates lipid peroxidation by inhibiting GPX4. [23,24]. Mirroring the oxytosis results, compounds **16a** (Fig. 4E) and **22** (Fig. 4K) exhibited neuroprotective effects equivalent to compound **10** (Fig. 4B), with activity diminishing at

Table 1
Structures and Physicochemical Antioxidant Parameters of target compounds in DPPH and ORAC assay.

Compound	Structure	DPPH Radical Scavenging Activity EC_{50} [μM]	ORAC (Trolox equivalents)	Log $P_{o/w}$[c]	BBB + Probability[d]
Ferulic acid	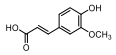	19.7 ± 0.5	3.2 ± 0.3	1.36	0.314
Caffeic acid	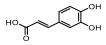	8.0 ± 0.5	4.8 ± 0.4	0.93	0.007
Trolox	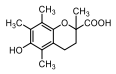	13.3 ± 2.6	–	2.47	0.986
Melatonin	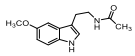	NA[a]	2.0 ± 0.3	1.83	0.989
Lipoic acid	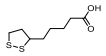	NA[a]	NA[a]	2.04	0.769
9		NA[a]	1.5 ± 0.2	1.07	1
10	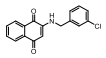	NA[a]	ND[b]	3.18	0.999
14	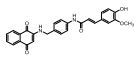	29.0 ± 3.6	2.7 ± 0.3	3.31	0.909
16a	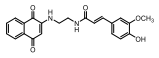	26.1 ± 1.5	3.1 ± 0.4	2.17	0.848
16b	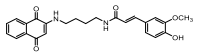	27.2 ± 2.9	2.2 ± 0.2	2.82	0.8
16c	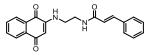	NA[a]	ND[b]	2.57	0.999
16d	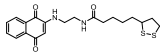	NA[a]	ND[b]	3.01	0.986
16e	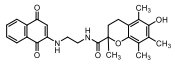	15.4 ± 1.9	1.6 ± 0.2	3.24	0.998
21	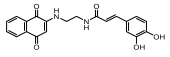	9.0 ± 0.7	3.5 ± 0.4	1.81	0.232
22	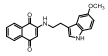	NA[a]	1.8 ± 0.2	3.05	0.98
24	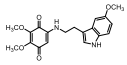	NA[a]	3.0 ± 0.4	1.94	0.107
25	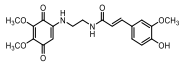	28.4 ± 1.2	3.5 ± 0.5	1.07	0.006

[a] Not active.
[b] Not determined due to interference from their own fluorescence.
[c] Log $P_{o/w}$ was predicted by the SwissADME online server [22].
[d] The probabilities of crossing the blood-brain barrier were predicted by Deep-PK online server: https://biosig.lab.uq.edu.au/deeppk/.

concentrations ≤1.56 μM. Notably, compound **16e** retained potent neuroprotection even at 0.38 μM (Fig. 4H).

The ATP depletion model employs iodoacetic acid (IAA), an irreversible inhibitor of glyceraldehyde 3-phosphate dehydrogenase (GAPDH), to induce glycolytic impairment and energy failure in HT22 cells, and has been commonly used in screens for neuroprotective compounds [8,25]. As shown in Fig. 4C–F, and L, compounds **10**, **16a**, and **22** displayed similar efficacy against IAA-induced injury. Compound **16e** again demonstrated superior activity, maintaining significant protection at 0.38 μM (Fig. 4I).

Collectively, multi-parametric assessment across oxytosis, ferroptosis, and ATP depletion assays revealed that compounds **16a** and **22** exhibit neuroprotective activity comparable to reference **10**. Strikingly, compound **16e** demonstrated significantly enhanced neuroprotective efficacy at sub-micromolar concentrations relative to compound **10**, indicating that hybridization with the Trolox pharmacophore conferred superior therapeutic potential.

2.5. Evaluation of synergistic effects and cytotoxicity profiles

The exceptional neuroprotective potency of compound **16e** in ferroptosis and ATP depletion assays prompted investigation into potential synergistic interactions between vitamin K derivatives and Trolox. To evaluate this, compound **9** served as a reference for comparing **16e**

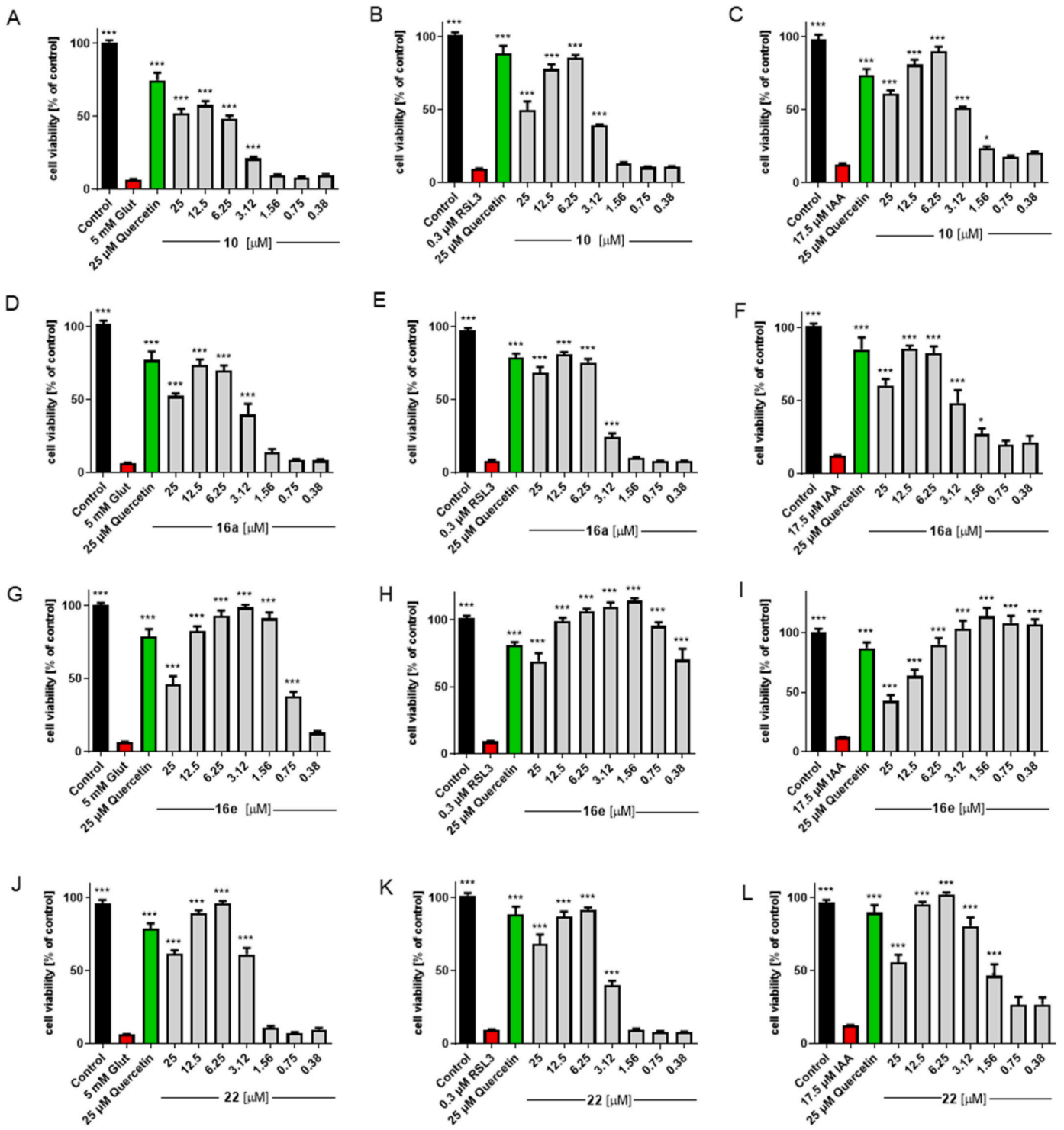

Fig. 4. Neuroprotection of compounds **10**, **16a**, **16e**, and **22** at 0.38–25 μM against 5 mM glutamate induced oxytosis (A, D, G, J), 0.3 μM RSL3 induced ferroptosis (B, E, H, K), and 17.5 μM iodoacetic acid (IAA) induced ATP depletion (C, F, I, L) in HT22 hippocampal nerve cells. Data is presented as means ± SEM of three independent experiments and results refer to untreated control cells (black). Statistical analysis was rendered using One-way ANOVA followed by Dunnett's multiple comparison post-hoc test referring to cells treated with 5 mM glutamate (A, D, G, J), 0.3 μM RSL3 (B, E, H, K) or 17.5 μM IAA (C, F, I, L). Levels of significance: $*p < 0.05$, $**p < 0.01$, $***p < 0.001$.

against an equimolar mixture of **9** and Trolox.

In the ferroptosis assay (Fig. 5), compound **9** demonstrated significant protection ≥1.56 μM, with reduced cell viability at 25 μM indicative of possible neurotoxic liability (Fig. 5B). Trolox alone showed no activity at 0.38–25 μM (Fig. 5A). Conversely, the **9**/Trolox mixture exhibited potent neuroprotection from 0.15 μM (Fig. 5C), significantly exceeding the potency of compound **9** alone. This marked enhancement suggests synergistic protection against RSL3-induced ferroptosis in HT22 cells. Compound **16e** (Fig. 5D) displayed protection comparable to the **9**/Trolox mixture across all concentrations, confirming retention of synergy within the hybrid scaffold. Crucially, compound **16e** offers inherent advantages over combination therapy—including lower

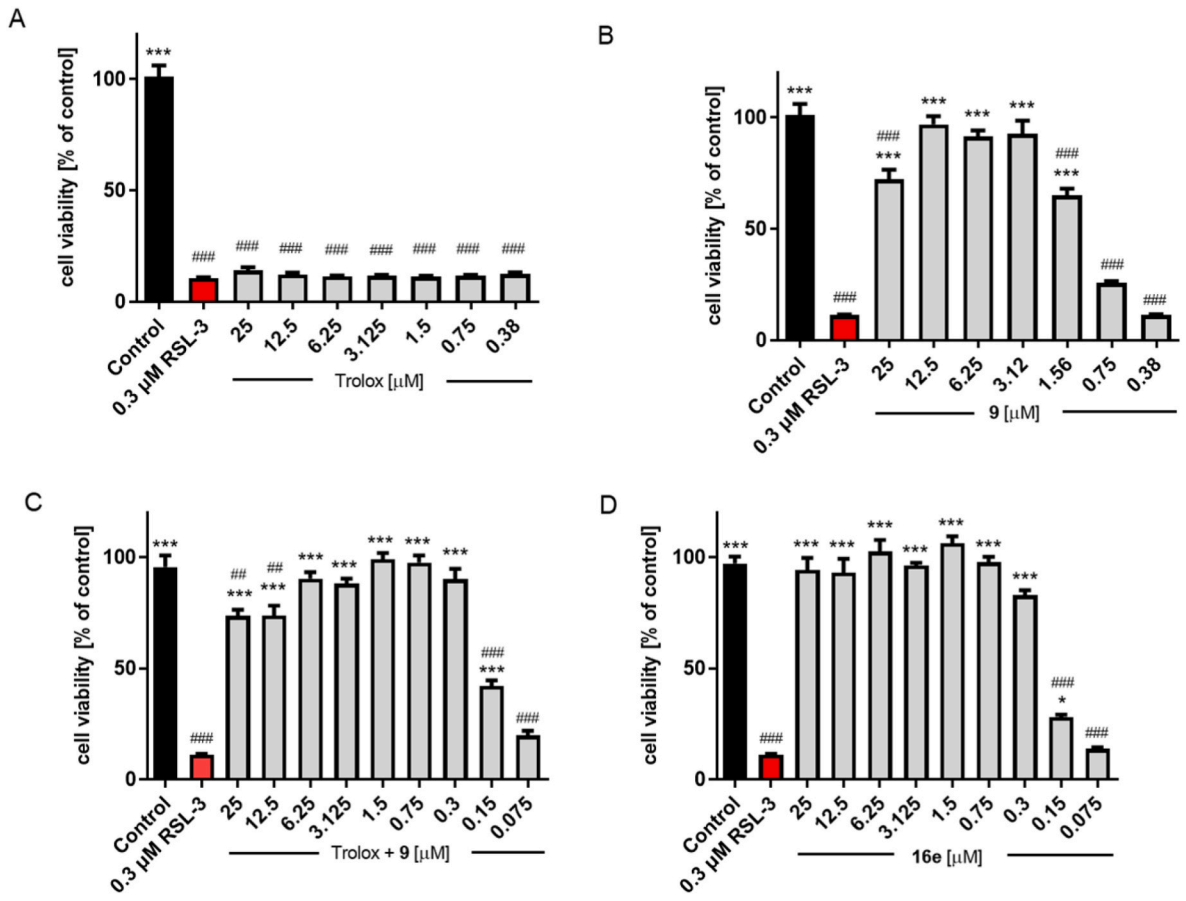

Fig. 5. Neuroprotective effects of compound **16e** and the controls 2-amino-1,4-naphthoquinone (**9**), Trolox, and the equimolar mixture of **9** and Trolox (Trolox + **9**) in ferroptosis assay at 0.075–25 μM. Data is presented as means ± SEM of three independent experiments and results refer to untreated control cells (black). Statistical analysis was rendered using One-way ANOVA followed by Dunnett's multiple comparison post-hoc test. $^{*}p < 0.05$, $^{**}p < 0.01$, $^{***}p < 0.001$ vs 0.3 μM RSL3 treated group (red). $^{\#}p < 0.01$, $^{\#\#}p < 0.01$, $^{\#\#\#}p < 0.001$ vs control group. (For interpretation of the references to colour in this figure legend, the reader is referred to the Web version of this article.)

neurotoxicity (Fig. 6), a streamlined pharmacokinetic profile, reduced ADMET complexity, and elimination of drug-drug interaction risks.

In the IAA-induced ATP depletion assay (Fig. S1), Trolox showed modest but significant protection ≥1.5 μM. Compounds **9**, **16e**, and the **9**/Trolox mixture exhibited high potency down to 0.075 μM. Notably, compound **9** and the mixture displayed significant cytotoxicity at ≥12.5 μM, whereas **16e** maintained protection with only marginal viability reduction at 25 μM.

Compound **16e**, the most potent hybrid identified, demonstrates pronounced antioxidant activity and neuroprotection at sub-micromolar concentrations (oxytosis: 0.75 μM; ferroptosis: 0.15 μM; ATP depletion: 0.075 μM). While synergistic neuroprotection between Trolox and vitamin K derivative **9** was established in ferroptosis, **16e** not only preserves this synergy but significantly mitigates the neurotoxic liability associated with the parent scaffold and its physical mixture.

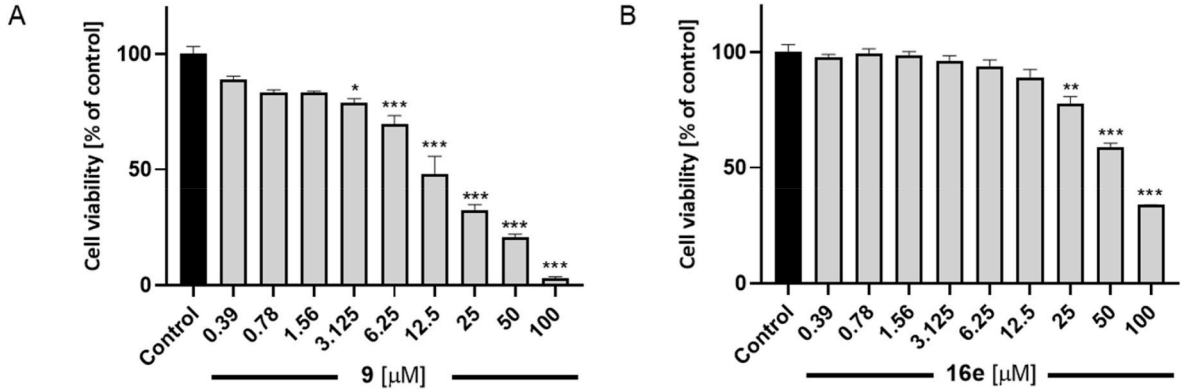

Fig. 6. Cytotoxicities of compounds **9** (A) and **16e** (B) in HT22 cells. Data is presented as means ± SEM of three independent experiments. Statistical analysis was rendered using One-way ANOVA followed by Dunnett's multiple comparison post-hoc test. $^{*}p < 0.05$, $^{**}p < 0.01$, $^{***}p < 0.001$ vs Control group.

2.6. Intracellular reactive oxygen species (ROS) measurement

ROS accumulation, a hallmark event in glutamate-induced oxytosis, occurs 6–8 h following inhibition of the cystine/glutamate antiporter (system Xc-) by high glutamate concentrations. Utilizing the fluorogenic probe H_2DCFDA, which emits intense fluorescence upon oxidation by ROS, we assessed the ability of compounds **9** and **16e** to attenuate ROS accumulation in this model. As shown in Fig. 7, both compounds **9** and **16e** (0.4 μM) significantly suppressed ROS generation. These findings suggest that their neuroprotective effects involve mitigation of oxidative stress via inhibition of ROS accumulation.

2.7. Immunomodulatory effect

Microglial overactivation is a hallmark of neuroinflammation and a known contributor to neurodegenerative pathologies, including Alzheimer's disease. While menaquinone-4 (MK-4), a vitamin K2 subtype, has demonstrated anti-inflammation effects in LPS-induced models [26,27], we investigated the potential of hybrid compound **16e**, Trolox, and vitamin K derivatives **9** and **10** to modulate microglial phenotype. Specifically, we assessed their ability to shift N9 microglia from a neurotoxic, LPS-induced M1 state – characterized by IL-1β release and iNOS expression – towards a neuroprotective M2 phenotype, marked by TREM2 and TGFβ2. As shown in Fig. 8, compound **16e** dose-dependently suppressed nitrite accumulation and IL-1β release, exhibiting potency comparable to Trolox but lower than compounds **9** and **10**. Furthermore, **16e** significantly attenuated LPS-induced iNOS protein upregulation, showing greater efficacy than Trolox, though less than compound **10**. In contrast, none of the tested compounds (**9**, **10**, Trolox, or **16e**) significantly modulated expression of the M2 markers TREM2 or TGFβ2. These data indicate that hybrid vitamin K compound **16e** possesses immunomodulatory activity by attenuating LPS-induced M1 microglial activation and its associated pro-inflammatory mediators (nitrite, IL-1β, iNOS). The reduced M1-suppressive potency of **16e** compared to its parent compound **10** suggests that Trolox hybridization may attenuate the anti-neuroinflammatory efficacy intrinsic to the vitamin K pharmacophore. Although no phenotypic shift toward the M2 state was observed, the selective suppression of M1 markers supports the anti-neuroinflammatory potential of compound **16e**.

2.8. Pan-assay interference compounds (PAINS) exclusion assay

Quinone-containing compounds possess a reactive Michael acceptor motif, rendering them susceptible to classification as pan-assay interference compounds (PAINS) by computational filters. Following the Chou group's methodology using 2-mercaptoethanol (BME) to confirm deactivation of the Michael acceptor via naphthoquinone amination [28], we evaluated thiol reactivity of our quinone hybrids in PBS (pH 7.4). As shown in Fig. S2, control compounds **11** (1,4-naphthoquinone; vitamin K core) and **23** (2,3-dimethoxy-5-methyl-1,4-benzoquinone; ubiquinone core) reacted completely with BME within 5 min. In stark contrast, hybrid compounds **16e** (vitamin K hybrid) and **25** (ubiquinone hybrid) exhibited no reactivity with BME over 6 h. This study confirms that amination effectively abolishes thiol reactivity in both naphthoquinone and ubiquinone scaffolds, eliminating a critical PAINS liability.

2.9. In vivo studies

Based on the potent anti-oxytosis/ferroptosis activity of compound **16e** in several *in vitro* assays, we evaluated its neuroprotective efficacy *in vivo* using an acute Alzheimer's disease mouse model induced by oligomerized $A\beta_{25-35}$ peptide [29,30]. The peptide was administered intracerebroventricularly (i.c.v.) on Day 1. Compounds **9** and **16e** were administered intraperitoneally (i.p.) daily from Days 1–7. Spatial short-term working memory was assessed via spontaneous alternation behavior in the Y-maze (Day 8). As shown in Fig. 9A and C, **16e** (0.1 mg/kg) significantly ameliorated $A\beta_{25-35}$-induced working memory deficits, surpassing the efficacy of compound **9** (active at 0.3 mg/kg). This demonstrates the enhanced *in vivo* potency of compound **16e**. Non-spatial long-term memory was evaluated using a passive avoidance paradigm with training on Day 9 and retention measured on Day 10. In contrast to the short-term memory results, neither compound **9** nor **16e** significantly ameliorated $A\beta_{25-35}$-induced long-term memory deficits at the tested doses. This observation will require further pharmacological analyses of the protective effect of the compounds *in vivo*, as short-term and long-term rely on different neurotransmission systems and brain neuronal structures. For instance, the drug effects on nitric oxide (NO)-related ROS must be explored as the NO/cyclic GMP system has been shown to play a selective role in spatial working memory deficits induced by *N*-methyl-D-aspartate receptors antagonists affecting spontaneous alternation behavior but not passive avoidance response [31].

3. Conclusions

In summary, we have successfully designed and synthesized ten novel neuroprotective hybrid compounds through the molecular hybridization of vitamin K derivatives with established antioxidants. Among these, the Trolox hybrid **16e** emerged as the lead candidate, demonstrating exceptional multi-pathway neuroprotective efficacy. Compound **16e** exhibited potent activity against glutamate-induced oxytosis in preliminary screening and achieved submicromolar inhibition of RSL3-induced ferroptosis ($IC_{50} = 0.22$ μM) alongside nanomolar-range protection against IAA-induced ATP depletion. Crucially,

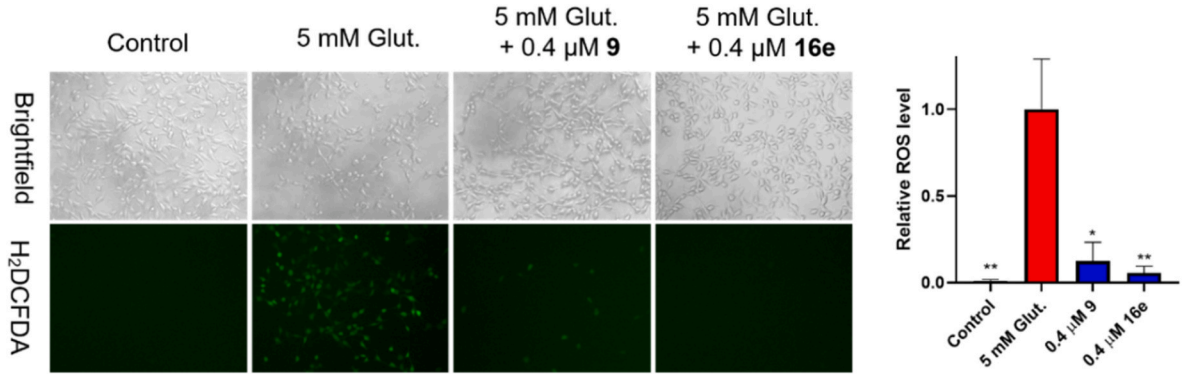

Fig. 7. Qualitative and quantitative analysis of formation of ROS with H_2DCFDA in HT22 cells. The cells were treated with or without glutamate for 8 h in the presence or absence of compounds **9** and **16e**. Data is presented as means ± SEM of three independent experiments. Statistical analysis was rendered using One-way ANOVA followed by Dunnett's multiple comparison post-hoc test. *$p < 0.05$, **$p < 0.01$, ***$p < 0.001$ vs 5 mM Glut. group.

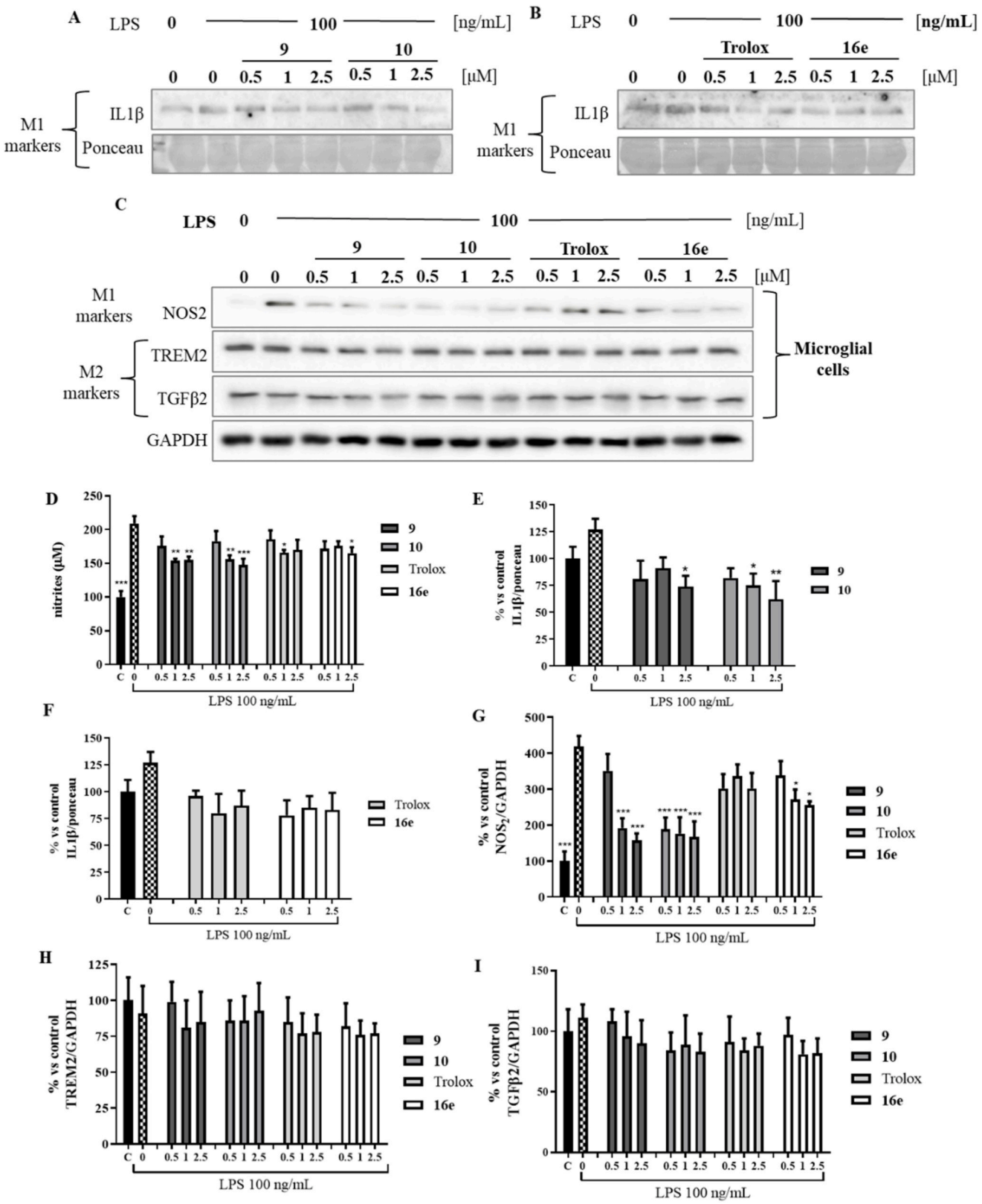

Fig. 8. Effect of compound **16e** and controls **9**, **10**, and Trolox on murine N9 cells induced in a M1 activation state by LPS (100 ng/mL) treatment. IL1β release (A, B, E and F) in N9-conditioned medium and expression of iNOS (C and G), TREM2 (C and H) and TGFβ2 (C and I) were analyzed by Western blot after 24 h treatment with LPS in presence of increasing concentrations (0.5, 1 and 2.5 μM) of compounds **9**, **10**, Trolox and compound **16e**. Nitric oxide release was evaluated through Griess reaction in media conditioned for 24 h by microglial cells treated with LPS in presence of compounds **9**, **10**, Trolox and **16e** (D). All quantitative data are presented as means ± SEM from at least 3 independent experiments. Statistical analysis was rendered using One-way ANOVA followed by Dunnett's post-hoc test. *$p < 0.05$; **$p < 0.01$ compared to LPS-treated control.

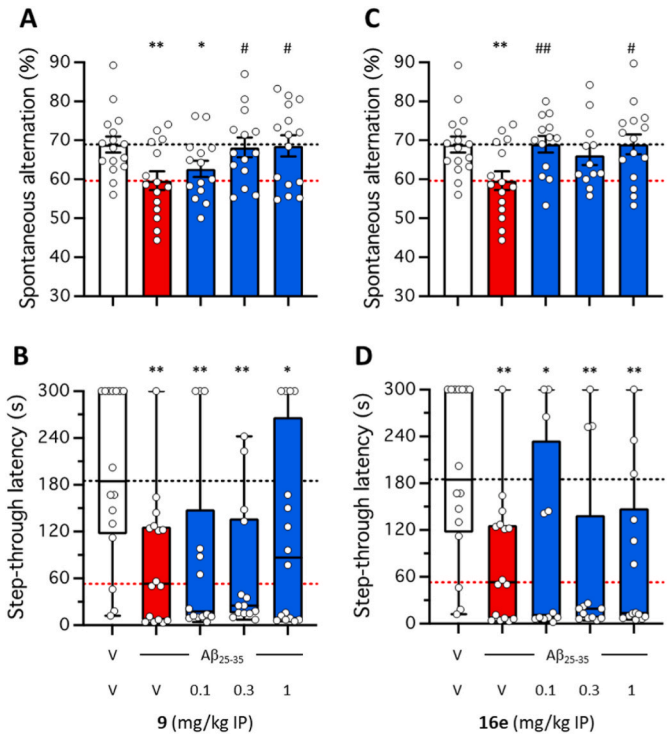

Fig. 9. Effects of compounds **9** (A, B) and **16e** (C, D) on A$\beta_{25\text{-}35}$ induced learning impairments in mice (A, C) Spontaneous alternation performance in the Y-maze and (B, D) retention latency in the passive avoidance test. N = 12–16 per group. Data show as means ± SEM (A, C) or median and interquartile range (B, D). *p < 0.05, **p < 0.01 vs V + V-treated group; #p < 0.05, ##p < 0.01 vs Aß$_{25\text{-}35}$+V-treated group; Dunnett's test in (A, C); Dunn's test in (B, D).

compound **16e** retained the pronounced synergistic neuroprotectivity observed with the combination of Trolox and vitamin K derivative **9** against ferroptosis, while displaying a superior safety profile with reduced cytotoxicity. This hybrid also manifested significant antioxidant capacity (DPPH EC_{50} = 15.4 μM, ORAC value 1.6) and immunomodulatory activity, effectively suppressing LPS-induced M1 microglial activation and associated inflammatory mediators. Importantly, the structural optimization via amination effectively ablated the inherent thiol reactivity associated with quinone cores, mitigating PAINS concerns as proved experimentally. Translating these *in vitro* benefits, compound **16e** demonstrated compelling *in vivo* efficacy in an established Alzheimer's disease mouse model, dose-dependently ameliorating Aβ$_{25\text{-}35}$-induced spatial working memory deficits at a low dose of 0.1 mg/kg – even outperforming parent compound **9** (active only at 0.3 mg/kg). Collectively, the rational hybridization strategy successfully integrated synergistic pharmacophores into a single entity, yielding compound **16e** as a promising, multi-mechanistic lead candidate with potent neuroprotection, antioxidant and immunomodulatory activities, favorable physicochemical properties, and demonstrable *in vivo* efficacy for further development against neurodegenerative diseases.

4. Experimental section

4.1. Chemistry

Common reagents and solvents were purchased from commercial suppliers and used without further purification unless otherwise stated. Tetrahydrofuran (THF) was distilled from sodium-benzophenone under an argon atmosphere. Reaction progress was monitored using analytical thin layer chromatography (TLC) on precoated silica gel GF254 plates (Macherey Nagel GmbH & Co. KG, Duren, Germany), and spots were detected under UV light (254 nm and 366 nm). Compounds were purified with flash column chromatography with a silica gel with a particle size of 40–63 μm (VWR chemicals, Leuven, Belgium) as the stationary phase and petroleum ether/ethyl acetate or dichloromethane/methanol mixtures as eluent systems. Nuclear magnetic resonance spectra were measured on a Bruker AV-400 NMR instrument (Bruker, Karlsruhe, Germany) in deuterated solvents (DMSO-d_6, $CDCl_3$, MeOD-d_4). Chemical shifts are expressed in ppm relative to DMSO-d_6, $CDCl_3$, or MeOD-d_4 (2.50/7.26/3.31 for ^{1}H; 39.52/77.16/49.00 for ^{13}C). Uncorrected melting points were measured using a Stuart melting point apparatus SMP30.

Measurements for verification and purity of the compounds were performed by LC/MS (from Shimadzu), comprising a DGU-20A3R controller, pump LC-20 A B, degasser DGU-20A, and SPD-20A UV/Vis detector. ESI ionization was accomplished by an LCMS-2020 single quadrupol mass spectrometer. As a stationary phase, for analytical purpose, a Synergi 4U fusion-RP 80 Å (150 × 4.6 mm) column and for preparative purpose, a Synergi 4U fusion-RP 80 Å (250 × 10.0 mm) were used. As a mobile phase, a gradient of MeOH/water (both containing 0.1 % formic acid) (phase 1/phase 2) was used. The compounds were dissolved in MeOH and filtered through syringe filters. Method: V(1)/(V(1) + V(2)) = from 5 to 90 % over 10 min, V(1)/(V(1) + V(2)) = 90 % for 5 min, V(1)/(V(1) + V(2)) = from 90 to 5 % over 3 min. Methods were performed with a flow rate of 1.0 mL/min. Compounds were detected at λ = 254 nm, and target compounds were ≥95 % pure.

4.1.1. 2-((4-Aminobenzyl)amino)naphthalene-1,4-dione (12)

4-(Aminomethyl)aniline (0.46 g, 3.79 mmol) was added to a solution of 1,4-naphthoquinone (0.60 g, 3.79 mmol) in ethanol, then stirred at room temperature for 1 h. The mixture was concentrated under vacuum and purified with column chromatography to afford red solid 0.42 g,. Brown solid, yield 40 %. ^{1}H NMR (400 MHz, $CDCl_3$): δ 8.12 (d, J = 7.7 Hz, 1H), 8.06 (d, J = 7.6 Hz, 1H), 7.74 (t, J = 7.3 Hz, 1H), 7.63 (t, J = 7.5 Hz, 1H), 7.13 (d, J = 8.3 Hz, 2H), 6.70 (d, J = 8.3 Hz, 2H), 6.10 (s, 1H), 5.83 (s, 1H), 4.25 (d, J = 5.5 Hz, 2H), 3.74 (s, 2H) ppm. ^{13}C NMR (101 MHz, $CDCl_3$): δ 183.0, 181.9, 147.7, 146.4, 134.7, 133.7, 132.0, 130.6, 129.2, 126.3, 126.2, 125.5, 115.4, 101.4, 46.6 ppm. LRMS (ESI+) m/z calcd for $[C_{17}H_{15}N_2O_2]^+$: 279.11, found: 279.10 $[M+H]^+$.

4.1.2. (E)-N-(4-(((1,4-Dioxo-1,4-dihydronaphthalen-2-yl)amino)methyl)phenyl)-3-(4-hydroxy-3-methoxyphenyl)acrylamide (13)

Triethylamine (0.55 g, 5.39 mmol) and ethyl chloroformate (0.35 g, 3.23 mmol) were added to a solution of ferulic acid (0.31 g, 1.62 mmol) in 20 mL THF at 0 °C and stirred for 10 min. Then intermediate **12** (0.30 g, 1.08 mmol) was added to the mixture and stirred at r.t. for 1 h. The mixture was concentrated under vacuum, then the residue was redissolved in DCM and washed with water and brine. The organic phase was dried over Na_2SO_4 and concentrated under vacuum to afford red solid. The red solid was then dissolved in methanol and KOH (0.12 g, 2.16 mmol) was added to the mixture. After stirring at r.t. for 10 min, the mixture was extracted with DCM and washed with water and brine. Dried over Na_2SO_4 and purified with column chromatography to afford red solid 75 mg, yield 15 %. ^{1}H NMR (400 MHz, DMSO-d_6): δ 10.08 (s, 1H), 9.51 (s, 1H), 8.13 (t, J = 6.4 Hz, 1H), 8.00 (d, J = 7.6 Hz, 1H), 7.91 (d, J = 7.6 Hz, 1H), 7.81 (t, J = 7.5 Hz, 1H), 7.73 (t, J = 7.5 Hz, 1H), 7.66 (d, J = 8.3 Hz, 2H), 7.48 (d, J = 15.6 Hz, 1H), 7.31 (d, J = 8.3 Hz, 2H), 7.18 (s, 1H), 7.06 (d, J = 8.1 Hz, 1H), 6.82 (d, J = 8.1 Hz, 1H), 6.63 (d, J = 15.6 Hz, 1H), 5.59 (s, 1H), 4.41 (d, J = 6.3 Hz, 2H), 3.83 (s, 3H) ppm. ^{13}C NMR (101 MHz, DMSO-d_6): δ 182.1, 181.8, 164.4, 149.1, 148.9, 148.3, 141.1, 139.0, 135.3, 133.5, 132.7, 132.4, 130.9, 128.1 (2C), 126.7, 126.4, 125.8, 122.5, 119.7 (2C), 119.3, 116.2, 111.3, 100.9, 56.0, 45.3 ppm. LRMS (ESI+) m/z calcd for $[C_{27}H_{23}N_2O_5]^+$: 455.15, found: 455.10 $[M+H]^+$. HPLC: t_R = 12.1 min, purity 96.4 %. mp = 209–210 °C.

4.1.3. (E)-N-(2-((1,4-Dioxo-1,4-dihydronaphthalen-2-yl)amino)ethyl)-3-(4-hydroxy-3-methoxyphenyl)acrylamide (16a)

TEA (0.48 g, 4.74 mmol) and HBTU (0.66 g, 1.73 mmol) were added

to a solution of ferulic acid (0.31 g, 1.58 mmol) in 20 mL DCM and stirred at room temperature for 1 h. The mixture was added dropwise to a solution of ethylenediamine (0.48 g, 7.97 mmol) in 10 mL DCM and stirred at room temperature for 1 h. The mixture was then concentrated under vacuum till the excess of ethylenediamine was removed. 1,4-Naphthoquinone (0.50 g, 3.16 mmol) in 20 mL ethanol was added to the residue and stirred for 1 h. The mixture was concentrated under vacuum and purified with column chromatography to afford orange solid 100 mg, yield 16 %. ^{1}H NMR (400 MHz, DMSO-d_6): δ 9.48 (s, 1H), 8.25 (t, J = 5.8 Hz, 1H), 8.07–8.02 (m, 1H), 8.02–7.96 (m, 1H), 7.88 (td, J = 7.5, 1.2 Hz, 1H), 7.78 (td, J = 7.5, 1.2 Hz, 1H), 7.65 (t, J = 5.8 Hz, 1H), 7.41 (d, J = 15.7 Hz, 1H), 7.18 (d, J = 1.7 Hz, 1H), 7.05 (dd, J = 8.2, 1.7 Hz, 1H), 6.84 (d, J = 8.1 Hz, 1H), 6.46 (d, J = 15.7 Hz, 1H), 5.86 (s, 1H), 3.86 (s, 3H), 3.47 (q, J = 6.0 Hz, 2H), 3.35 (q, J = 6.2 Hz, 2H) ppm. ^{13}C NMR (101 MHz, DMSO-d_6): δ 181.9, 166.6, 149.2, 148.8, 148.3, 139.9, 135.3, 133.6, 132.7, 130.8, 126.8, 126.3, 125.8, 122.1, 119.0, 116.1, 111.3, 100.1, 56.0, 42.7, 37.4 ppm. LRMS (ESI+) m/z calcd for $[C_{22}H_{21}N_2O_5]^+$: 393.14, found: 393.10 $[M+H]^+$. HPLC: t_R = 11.0 min, purity 95.9 %. mp = 194–196 °C.

4.1.4. (E)-N-(4-((1,4-Dioxo-1,4-dihydronaphthalen-2-yl)amino)butyl)-3-(3-hydroxy-4-methoxyphenyl)acrylamide (16 b)

Compound **16b** was prepared from ferulic acid, 1,4-butanediamine and 1,4-naphthoquinone in a similar manner as described for compound **16a**. Red solid, yield 3 %. ^{1}H NMR (400 MHz, DMSO-d_6): δ 9.40 (s, 1H), 8.02–7.91 (m, 3H), 7.82 (t, J = 7.5 Hz, 1H), 7.72 (t, J = 7.5 Hz, 1H), 7.57 (t, J = 6.0 Hz, 1H), 7.31 (d, J = 15.7 Hz, 1H), 7.11 (d, J = 1.4 Hz, 1H), 6.98 (dd, J = 8.1, 1.5 Hz, 1H), 6.79 (d, J = 8.1 Hz, 1H), 6.43 (d, J = 15.7 Hz, 1H), 5.71 (s, 1H), 3.80 (s, 3H), 3.27–3.13 (m, 4H), 1.70–1.56 (m, 2H), 1.56–1.46 (m, 2H) ppm. ^{13}C NMR (101 MHz, DMSO-d_6): δ 182.1, 181.7, 165.8, 149.0, 148.7, 148.3, 139.3, 135.3, 133.7, 132.6, 130.9, 126.9, 126.3, 125.8, 122.0, 119.5, 116.1, 111.2, 99.8, 56.0, 42.1, 38.8, 27.2, 25.4 ppm. LRMS (ESI+) m/z calcd for $[C_{24}H_{25}N_2O_5]^+$: 421.17, found: 421.10 $[M+H]^+$. HPLC: t_R = 14.1 min, purity 96.3 %. mp = 181–183 °C.

4.1.4.1. N-(2-((1,4-Dioxo-1,4-dihydronaphthalen-2-yl)amino)ethyl)cinnamamide (16c).

Compound **16c** was prepared from cinnamic acid, ethylenediamine and 1,4-naphthoquinone in a similar manner as described for compound **16a**. Brown solid, yield 16 %. ^{1}H NMR (400 MHz, DMSO-d_6): δ 8.35 (t, J = 5.8 Hz, 1H), 7.99 (dd, J = 7.7, 1.0 Hz, 1H), 7.94 (dd, J = 7.6, 1.0 Hz, 1H), 7.83 (td, J = 7.5, 1.3 Hz, 1H), 7.73 (td, J = 7.5, 1.3 Hz, 1H), 7.61 (t, J = 5.9 Hz, 1H), 7.58–7.55 (m, 2H), 7.46 (d, J = 15.8 Hz, 1H), 7.41 (d, J = 7.6 Hz, 2H), 7.39–7.37 (m, 1H), 6.60 (d, J = 15.8 Hz, 1H), 5.81 (s, 1H), 3.44 (q, J = 6.1 Hz, 2H), 3.31 (q, J = 6.1 Hz, 2H) ppm. ^{13}C NMR (101 MHz, DMSO-d_6): δ 181.9 (2C), 166.1, 149.2, 139.5, 135.3, 135.3, 133.6, 132.7, 130.8, 130.0, 129.4 (2C), 128.0 (2C), 126.3, 125.8, 122.3, 100.1, 42.6, 37.5 ppm. LRMS (ESI+) m/z calcd for $[C_{21}H_{19}N_2O_3]^+$: 347.13, found: 347.10 $[M+H]^+$. HPLC: t_R = 11.8 min, purity 99.8 %. mp = 226–228 °C.

4.1.5. N-(2-((1,4-Dioxo-1,4-dihydronaphthalen-2-yl)amino)ethyl)-5-(1,2-dithiolan-3-yl)pentanamide (16d)

Compound **16d** was prepared from 1,4-naphthquinone and lipoic acid in a similar manner as described for compound **16a**. Orange solid 24 mg, yield 3 %. ^{1}H NMR (400 MHz, DMSO-d_6): δ 8.10–7.90 (m, 3H), 7.89–7.79 (m, 1H), 7.73 (t, J = 6.8 Hz, 1H), 7.51 (s, 1H), 5.76 (s, 1H), 3.61–3.49 (m, 1H), 3.26–3.19 (m, 2H), 3.19–3.11 (m, 1H), 3.11–3.02 (m, 1H), 2.42–2.29 (m, 1H), 2.06 (t, J = 5.9 Hz, 2H), 1.90–1.74 (m, 1H), 1.68–1.56 (m, 1H), 1.56–1.22 (m, 7H) ppm. ^{13}C NMR (101 MHz, DMSO-d_6): δ 181.9, 173.2, 149.2, 147.7, 135.3, 133.6, 132.7, 130.8, 126.3, 125.8, 100.0, 56.5, 46.0, 42.6, 38.5, 37.3, 35.7, 34.6, 28.7, 25.4 ppm. LRMS (ESI+) m/z calcd for $[C_{20}H_{25}N_2O_3S_2]^+$: 405.12 found: 405.05 $[M+H]^+$. HPLC: t_R = 10.6 min, purity 95.6 %. mp = 164–165 °C.

4.1.6. N-(2-((1,4-Dioxo-1,4-dihydronaphthalen-2-yl)amino)ethyl)-6-hydroxy-2,5,7,8-tetramethylchromane-2-carboxamide (16e)

Compound **16e** was prepared from Trolox, ethylenediamine and 1,4-naphthoquinone in a similar manner as described for compound **16a**. Orange solid 43 mg, yield 48 %. ^{1}H NMR (400 MHz, $CDCl_3$): δ 8.10 (dd, J = 7.7, 0.7 Hz, 1H), 8.08–8.04 (m, 1H), 7.74 (td, J = 7.6, 1.3 Hz, 1H), 7.64 (td, J = 7.6, 1.2 Hz, 1H), 6.75 (t, J = 6.1 Hz, 1H), 6.26 (s, 1H), 5.64 (s, 1H), 3.79–3.62 (m, 1H), 3.54–3.41 (m, 2H), 3.27–3.18 (m, 2H), 2.69–2.48 (m, 2H), 2.47–2.36 (m, 1H), 2.14 (s, 3H), 2.11 (s, 3H), 2.03 (s, 3H), 1.92–1.83 (m, 1H), 1.55 (s, 3H) ppm. ^{13}C NMR (101 MHz, $CDCl_3$): δ 183.0, 181.3, 175.9, 148.2, 145.7, 144.1, 134.7, 133.5, 132.1, 130.5, 126.3, 126.2, 121.8, 121.7, 119.3, 118.0, 100.8, 78.4, 43.3, 37.6, 29.6, 24.7, 20.5, 12.2, 12.0, 11.3 ppm. LRMS (ESI+) m/z calcd for $[C_{26}H_{29}N_2O_5]^+$: 449.20, found: 449.10 $[M+H]^+$. HPLC: t_R = 12.0 min, purity 96.9 %.

4.1.7. (E)-3-(3,4-diacetoxyphenyl)acrylic acid (17)

Acetic anhydride (0.56 g, 5.50 mmol) was added to a solution of caffeic acid (0.10 g, 0.55 mmol) in 5 mL pyridine and stirred at r.t. Over night. The mixture was neutralized to pH 6, then excess water was added and extracted with DCM. The organic phase was combined and washed with water and brine, dried over Na_2SO_4 and concentrated under vacuum to afford white solid 0.12 g, yield 83 %. ^{1}H NMR (400 MHz, DMSO-d_6): δ 12.46 (s, 1H), 7.68–7.61 (m, 2H), 7.58 (d, J = 16.0 Hz, 1H), 7.32 (d, J = 8.3 Hz, 1H), 6.54 (d, J = 16.0 Hz, 1H), 2.30 (s, 3H), 2.29 (s, 3H) ppm. ^{13}C NMR (101 MHz, DMSO-d_6): δ 168.7, 168.6, 167.8, 143.8, 142.8, 142.6, 133.6, 127.2, 124.6, 123.5, 120.8, 20.8, 20.8 ppm. LRMS (ESI+) m/z calcd for $[C_{13}H_{13}O_6]^+$: 265.06 found: 265.00 $[M+H]^+$. HPLC: t_R = 10.4 min.

4.1.8. (E)-4-(3-((2-((tert-butoxycarbonyl)amino)ethyl)amino)-3-oxoprop-1-en-1-yl)-1,2-phenylene diacetate (18)

TEA (0.38 g, 3.79 mmol) and ethyl chloroformate (0.20 g, 1.89 mmol) were added to a solution of intermediate **17** (0.50 g, 1.89 mmol) in 20 mL THF and stirred at 0 °C for 10 min *tert*-Butyl (2-aminoethyl) carbamate (0.36 g, 2.27 mmol) prepared from ethylenediamine, Boc_2O, and TFA was added to the mixture and stirred at r.t. for 1 h. The mixture was concentrated under vacuum and purified with column chromatography to afford white solid 0.68 g, yield 88 %. ^{1}H NMR (400 MHz, $CDCl_3$): δ 7.55 (d, J = 15.6 Hz, 1H), 7.37 (dd, J = 8.4, 1.9 Hz, 1H), 7.33 (d, J = 1.8 Hz, 1H), 7.20 (d, J = 8.3 Hz, 1H), 6.60 (s, 1H), 6.34 (d, J = 15.6 Hz, 1H), 5.06 (s, 1H), 3.53–3.46 (m, 2H), 3.41–3.28 (m, 2H), 2.32 (s, 3H), 2.31 (s, 3H), 1.46 (s, 9H) ppm. ^{13}C NMR (101 MHz, $CDCl_3$): δ 168.1, 168.1, 166.1, 155.23143.0, 142.4, 139.1, 133.8, 126.1, 123.8, 122.4, 121.9, 79.9, 50.8 (2C), 28.4 (3C), 20.7, 20.6 ppm. LRMS (ESI+) m/z calcd for $[C_{20}H_{27}N_2O_7]^+$: 407.17 found: 407.15 $[M+H]^+$. HPLC: t_R = 10.7 min.

4.1.9. (E)-4-(3-((2-((1,4-dioxo-1,4-dihydronaphthalen-2-yl)amino)ethyl)amino)-3-oxoprop-1-en-1-yl)-1,2-phenylene diacetate (20)

1 mL TFA was added dropwise to a solution of intermediate **18** (0.20 g, 0.50 mmol) in 10 mL DCM and stirred at r.t. for 30 min. The mixture was concentrated under vacuum to afford crude intermediate **19**. Intermediate **19** and TEA (51 mg, 0.50 mmol) were added to a solution of 1,4-naphthoquinone (0.16 g, 1.00 mmol) in 5 mL DCM and stirred at r.t. for 30 min. The mixture was concentrated under vacuum and purified with column chromatography to afford intermediate orange solid 0.18 g, yield 79 %. ^{1}H NMR (400 MHz, DMSO-d_6): δ 8.35 (t, J = 5.7 Hz, 1H), 7.99 (d, J = 7.5 Hz, 1H), 7.95 (d, J = 7.5 Hz, 1H), 7.83 (td, J = 7.5, 1.0 Hz, 1H), 7.73 (td, J = 7.5, 1.0 Hz, 1H), 7.61 (t, J = 5.9 Hz, 1H), 7.54–7.48 (m, 2H), 7.45 (d, J = 15.8 Hz, 1H), 7.31 (d, J = 8.2 Hz, 1H), 6.58 (d, J = 15.8 Hz, 1H), 5.82 (s, 1H), 3.43 (dd, J = 12.0, 6.0 Hz, 2H), 3.33–3.27 (m, 2H), 2.30 (s, 3H), 2.29 (s, 3H) ppm. ^{13}C NMR (101 MHz, DMSO-d_6): δ 181.9, 168.7, 168.6, 165.9, 149.2, 143.2, 142.8, 137.8, 135.3, 134.2, 133.8, 133.6, 132.7, 130.9, 126.4, 126.3, 125.8, 124.6, 123.4, 122.8, 100.2, 42.5, 37.5, 20.82, 20.81 ppm. LRMS (ESI+) m/z

calcd for $[C_{25}H_{23}N_2O_7]^+$: 463.14 found: 463.05 $[M+H]^+$. HPLC: t_R = 11.3 min.

4.1.10. (E)-3-(3,4-dihydroxyphenyl)-N-(2-((1,4-dioxo-1,4-dihydronaphthalen-2-yl)amino)ethyl)acrylamide (21)

KOH (64 mg, 1.14 mmol) in 2 mL methanol was added dropwise to a solution of intermediate **20** (0.26 g, 0.57 mmol) in 8 mL methanol and stirred at r.t. for 10 min. The mixture was acidified to pH 4 and concentrated under vacuum. The raw product was purified with column chromatography to afford orange solid 55 mg, yield 26 %. ^{1}H NMR (400 MHz, DMSO-d_6): δ 9.41 (s, 1H), 9.18 (s, 1H), 8.31 (t, J = 5.7 Hz, 1H), 8.02–7.97 (m, 1H), 7.96–7.91 (m, 1H), 7.83 (td, J = 7.5, 1.1 Hz, 1H), 7.73 (td, J = 7.5, 1.1 Hz, 1H), 7.62 (t, J = 5.8 Hz, 1H), 7.28 (d, J = 15.7 Hz, 1H), 6.97 (d, J = 1.9 Hz, 1H), 6.85 (dd, J = 8.2, 1.8 Hz, 1H), 6.76 (d, J = 8.1 Hz, 1H), 6.31 (d, J = 15.7 Hz, 1H), 5.80 (s, 1H), 3.41 (dd, J = 11.8, 5.9 Hz, 2H), 3.30 (dd, J = 11.8, 5.9 Hz, 2H) ppm. ^{13}C NMR (101 MHz, DMSO-d_6): δ 181.9, 181.9, 166.7, 149.2, 147.9, 146.0, 140.0, 135.3, 133.6, 132.7, 130.9, 126.7, 126.4, 125.8, 120.9, 118.5, 116.3, 114.4, 100.1, 42.7, 37.4 ppm. LRMS (ESI+) *m/z* calcd for $[C_{21}H_{19}N_2O_5]^+$: 379.12 found: 379.05 $[M+H]^+$. HPLC: t_R = 10.5 min, purity = 97.9 %. mp = 259–261 °C.

4.1.11. 2-((2-(5-methoxy-1H-indol-3-yl)ethyl)amino)naphthalene-1,4-dione (22)

Compound **22** was prepared from 5-methoxytryptamine and 1,4-naphthoquinone in a similar manner as described for intermediate **12**. Red solid, yield 8 %. ^{1}H NMR (400 MHz, $CDCl_3$): δ 8.01 (dd, J = 7.7, 1.2 Hz, 2H), 7.92 (dd, J = 7.7, 1.2 Hz, 1H), 7.63 (td, J = 7.6, 1.3 Hz, 1H), 7.51 (td, J = 7.5, 1.2 Hz, 1H), 7.18 (d, J = 1.2 Hz, 1H), 6.97 (d, J = 2.0 Hz, 1H), 6.94 (d, J = 2.3 Hz, 1H), 6.80 (dd, J = 8.8, 2.4 Hz, 1H), 5.95 (s, 1H), 5.70 (s, 1H), 3.78 (s, 3H), 3.41 (q, J = 6.6 Hz, 2H), 3.03 (t, J = 6.8 Hz, 2H) ppm. ^{13}C NMR (101 M Hz, $CDCl_3$): δ 183.0, 181.8, 154.2, 147.9, 134.7, 133.7, 131.9, 131.6, 130.5, 127.4, 126.2, 126.2, 123.0, 112.7, 112.2, 111.8, 100.9, 100.3, 55.9, 42.5, 24.2 ppm. LRMS (ESI+) *m/z* calcd for $[C_{21}H_{19}N_2O_3]^+$: 347.13, found: 347.10 $[M+H]^+$. HPLC: t_R = 12.1 min, purity 95.9 %. mp = 166–167 °C.

4.1.12. 2,3-Dimethoxy-5-((2-(5-methoxy-1H-indol-3-yl)ethyl)amino)cyclohexa-2,5-diene-1,4-dione (24)

Compound **24** was prepared from 2,3-dimethoxycyclohexa-2,5-diene-1,4-dione and 5-methoxytryptamine in a similar manner as described for intermediate **12**. Brown solid 23 mg, yield 5 %. ^{1}H NMR (400 MHz, $CDCl_3$): δ 8.17 (s, 1H), 7.29 (d, J = 8.8 Hz, 1H), 7.05 (d, J = 2.2 Hz, 1H), 7.01 (d, J = 2.2 Hz, 1H), 6.90 (dd, J = 8.8, 2.4 Hz, 1H), 5.94 (s, 1H), 5.35 (s, 1H), 4.17 (s, 3H), 3.89 (s, 3H), 3.84 (s, 3H), 3.42 (q, J = 6.6 Hz, 2H), 3.08 (t, J = 6.8 Hz, 2H) ppm. ^{13}C NMR (101 MHz, $CDCl_3$): δ 181.3, 180.4, 154.2, 148.6, 145.8, 140.3, 131.6, 127.4, 123.0, 112.6, 112.2, 111.6, 100.3, 95.1, 61.4, 61.1, 56.0, 42.7, 24.1 ppm. LRMS (ESI+) *m/z* calcd for $[C_{19}H_{21}N_2O_5]^+$: 357.14 found: 357.05 $[M+H]^+$. HPLC: t_R = 10.7 min, purity 97.6 %. mp = 108–110 °C.

4.1.13. (E)-N-(2-((4,5-dimethoxy-3,6-dioxocyclohexa-1,4-dien-1-yl)amino)ethyl)-3-(4-hydroxy-3-methoxyphenyl)acrylamide (25)

Compound **25** was prepared from 2,3-dimethoxycyclohexa-2,5-diene-1,4-dione and ferulic acid in a similar manner as described for compound **16a**. Purple solid 40 mg, yield 6 %. ^{1}H NMR (400 MHz, DMSO-d_6): δ 9.46 (brs, 1H), 8.24–8.10 (m, 1H), 7.44 (t, J = 5.9 Hz, 1H), 7.35 (d, J = 15.7 Hz, 1H), 7.13 (d, J = 1.8 Hz, 1H), 7.00 (dd, J = 8.2, 1.8 Hz, 1H), 6.80 (d, J = 8.1 Hz, 1H), 6.40 (d, J = 15.7 Hz, 1H), 5.33 (s, 1H), 4.00 (s, 3H), 3.81 (s, 3H), 3.76 (s, 3H), 3.35 (q, J = 6.1 Hz, 2H), 3.19 (q, J = 6.1 Hz, 2H) ppm. ^{13}C NMR (101 MHz, DMSO-d_6): δ 180.6, 180.6, 166.6, 148.8, 148.4, 148.3, 147.0, 141.1, 139.9, 126.7, 122.1, 119.0, 116.1, 111.3, 94.5, 61.3, 61.1, 56.0, 42.8, 37.4 ppm. LRMS (ESI+) *m/z* calcd for $[C_{20}H_{23}N_2O_7]^+$: 403.14 found: 403.05 $[M+H]^+$. HPLC: t_R = 9.8 min, purity 97.9 %. mp = 75–77 °C.

4.2. DPPH assay

The DPPH assay was performed as previously described [32]. Briefly, a 200 μM DPPH stock solution was freshly prepared in methanol. Test compounds were dissolved in methanol (5 mM stock) and serially diluted. For each reaction, 50 μL of DPPH solution was added to 100 μL of diluted compound or methanol (negative control) in a 96-well plate. After 30 min incubation in darkness at room temperature, absorbance was measured at 517 nm using a microplate reader. Compound-specific blanks (dilution series without DPPH) were subtracted from corresponding measurements. All experiments were performed in triplicate. Radical scavenging potency was expressed as EC_{50} (concentration scavenging 50 % DPPH radicals) determined by nonlinear regression analysis.

4.3. Oxygen radical absorbance capacity (ORAC) assay

The ORAC assay was performed according to Ou et al. [33] with modifications by Dávalos et al. [34], using fluorescein (FL) as the fluorescent probe, Trolox as the standard, and 2,2′-azobis(2-methylpropionamidine) dihydrochloride (AAPH) as the peroxyl radical generator. Reactions were conducted in 75 mM phosphate buffer (pH 7.4, final volume 200 μL) at 37 °C. In black 96-well plates, 20 μL of test compound (final concentrations: 2 and 4 μM) or Trolox standard (1–15 μM) was mixed with 120 μL FL (70 nM final). After 15 min pre-incubation at 37 °C, 60 μL AAPH (12 mM final) was added to initiate oxidation. Fluorescence decay (λ_{ex} 485 nm, λ_{em} 510 nm) was monitored every 2 min for 90 min. The area under the curve (AUC) was calculated as:

$$AUC = 1 + \sum_{i=1}^{i=45} f_i \Big/ f_0$$

where f_0 = initial fluorescence (0 min) and f_i = fluorescence at time i. Net AUC (AUC_{sample} - AUC_{blank}) was plotted against Trolox concentration to generate a linear standard curve ($R^2 > 0.99$). ORAC values were expressed as Trolox equivalents, with pure Trolox defined as 1.0. All samples were analyzed in duplicate across three independent experiments.

4.4. Cell culture and viability assessment

HT22 cells were maintained in Dulbecco's Modified Eagle Medium (DMEM; Sigma-Aldrich) supplemented with 10 % (v/v) heat-inactivated fetal bovine serum (FBS) and 1 % (v/v) penicillin-streptomycin at 37 °C with 5 % CO_2 in a humidified incubator. Cells were subcultured every 48 h. For assays, cells were seeded in 96-well plates (3×10^3 cells/well) and incubated for 24 h.

For neurotoxicity assay, cells were exposed to diluted compounds or vehicle control (0.05 % DMSO) for 24 h. Viability was assessed using the MTT assay. Briefly, after compound removal, cells were incubated with MTT solution (0.4 mg/mL) for 3 h. Formazan crystals were dissolved in DMSO, and absorbance was measured at 560 nm. Data represent mean viability (%) relative to untreated controls ± SD (n = 3 independent experiments).

For oxytosis assay, cells were co-treated with 5 mM glutamate with diluted compounds for 24 h. Quercetin (25 μM) served as positive control. Viability was quantified via MTT assay.

For ferroptosis assay, cells were exposed to 0.3 μM RSL3 with diluted compounds for 24 h. Viability was assessed by MTT.

For ATP depletion assay, seeded cells were exposed to 17.5 μM iodoacetic acid (IAA) with diluted compounds for 2 h. Medium was replaced with fresh compound-containing medium (without IAA) for an additional 24 h before MTT analysis.

Cell viabilities are expressed as mean ± SEM. Significance was determined by one-way ANOVA with Dunnett's post-hoc test (*$p < 0.05$,

**p < 0.01, ***p < 0.001) using GraphPad Prism 7.

4.5. Intracellular ROS measurement and imaging

Intracellular reactive oxygen species (ROS) accumulation was quantified using the membrane-permeant fluorogenic probe 2′,7′-dichlorodihydrofluorescein diacetate (H_2DCFDA, Aladdin). HT-22 cells were seeded in 96-well plates (5×10^3 cells/well in 100 μL complete medium) and incubated overnight (37 °C, 5 % CO_2). Cells were then treated with 100 μL medium containing 5 mM glutamate (monosodium L-glutamate; Sigma-Aldrich) and test compounds and incubated for 8 h (37 °C, 5 % CO_2). H_2DCFDA (10 μM final concentration) was added and incubated for 20 min. Following two washes with serum-free medium, cells were maintained in 100 μL fresh medium for immediate imaging. Fluorescence imaging of oxidized dichlorofluorescein (DCF) was performed using a Nikon ECLIPSE Ti with a 10 × objective and FITC filters. All images were acquired with identical parameters (exposure time, gain, contrast). Quantification was performed in ImageJ (NIH) using consistent thresholding and analysis settings across treatment groups.

4.6. Pan-assay interference compounds (PAINS) exclusion assay

Thiol reactivity was assessed by incubating quinone derivatives (100 μM) with 2-mercaptoethanol (BME, 1 mM) in PBS (pH 7.4) at 25 °C. Reaction mixtures were analyzed by LCMS at 0 min, 5 min, and 6 h. Controls included vitamin K core **11** and ubiquinone core **23**.

4.7. Microglial immunomodulation assay

Mouse N9 microglial cells were cultured in DMEM supplemented with 10 % heat-inactivated FBS, 1 % penicillin/streptomycin, and 2 mM L-glutamine. For immunomodulation studies, microglial cells were counted by using BLAUBRAND® Neubauer chamber and 2.5×10^5 cells/35 mm ø Petri dish were plated in complete DMEM medium w/o FBS and exposed to 100 ng/ml lipopolysaccharide (LPS) – which induces M1 activation – and compounds at indicated concentrations. After 24 h incubation (37 °C, 5 % CO_2), conditioned media were collected and nitrites formed by spontaneous oxidation of Nitric Oxide (NO) were spectrophotometrically detected based on the Griess assay. In parallel, microglial cells were collected in lysis buffer (1 % SDS, 50 mM Tris-HCL pH 7.4, 1 mM EDTA, 10 μl/ml protease and phosphatase inhibitors) and protein concentration determined via Lowry assay. Secreted proteins in conditioned media were concentrated using Microcon YM-3 filters (Millipore) and reconstituted in 4 × Loading buffer.

Western Blot Analysis. Media and cell lysate samples were resolved on 12.5 % SDS-PAGE gels (Bio-Rad) and transferred to nitrocellulose membranes (GE Healthcare). Membranes were blocked in PBS-0.1 % Tween-20 with 5 % non-fat dry milk (1 h, RT), then incubated overnight (4 °C) with primary antibodies. The next day, after 3 washes in PBS-0.1 % Tween-20 membranes were then incubated with HRP-linked secondary antibodies (horseradish peroxidase conjugated) for 90 min at RT in PBS-0.1 % Tween-20 with 5 % non-fat dry milk. Proteins were visualized by using the Clarity™ Western ECL Substrate (Bio-Rad) and detected using Bio-Rad Image Lab Software with a ChemiDoc™ imaging system (Bio-Rad). Western blot primary antibodies: IL-1β (1:1000; Cell Signalling Technology, Danvers, Massachusetts), iNOS (1:1000; Cell Signalling Technology), TREM2 (1:1000; Thermo Fisher Scientific, Waltham, Massachusetts, USA), TGFβ2 (1:1000; Abcam, Cambridge, UK), GAPDH (1:20000; Santa Cruz Biotechnology, Dallas, Texas, USA). HRP-linked secondary antibodies (horseradish peroxidase conjugated): Goat anti-Mouse (Jackson ImmunoResearch, West Grove, Pennsylvania, USA), Goat anti-Rabbit (Jackson ImmunoResearch).

Nitrite Quantification. Nitric oxide production was determined by measuring nitrite accumulation via Griess reaction. Conditioned media were mixed with sulfanilamide (5 mM final) in 1 % phosphoric acid, followed by NEDA (40 mM final). After 15 min incubation (dark, RT), absorbance was measured at 540 nm. Nitrite concentrations were calculated from a $NaNO_2$ standard curve.

Statistical Analysis. Data represent mean ± SEM (n ≥ 3 independent experiments). Significance was determined by One-way ANOVA (Dunnett's post-hoc). (GraphPad Prism v.6; *$p < 0.05$, **$p < 0.01$, ***$p < 0.001$).

4.8. In vivo neuroprotection assessment

All procedures complied with EU Directive 2010/63/EU and ARRIVE guidelines, approved by the French National Ethics Committee (APAFIS #1485–15034). Male Swiss mice (Janvier; 6-weeks-old, 31–36 g) were kept in a temperature- and humidity-controlled animal facility on a 12 h/12 h light/dark cycle (lights off at 07:00 p.m.) with ad libitum access to food/water at CECEMA (University of Montpellier; agreement #B-34-172-23).

Compound Administration. Test compounds were dissolved in DMSO (10 mg/mL stock) and diluted in saline (final: 60 % DMSO). Mice received daily intraperitoneal injections (days 1–7; 10 mL/kg). Vehicle controls received 60 % DMSO/saline.

$A\beta_{25\text{-}35}$ Administration. On day 1, mice were anesthetized (isoflurane, 2.5 %) and administered oligomerized $A\beta_{25\text{-}35}$ (9 nmol, i.c.v.) or vehicle (bidistilled water) using established protocols [29].

Y-Maze Spontaneous Alternation (Day 8). Spatial working memory was assessed in a gray PVC maze (three 40-cm arms). Mice freely explored for 8 min while recording arm entry sequences. Alternation percentage = [successive entries into three different arms/(total entries - 2)] × 100. Animals with alternation <20 % or >90 %, or total entries <10 were excluded (5 mice/119).

Passive Avoidance (Days 9-10). Long-term memory was evaluated in a two-chamber apparatus (light/dark compartments). On day 9 (training), mice entering the dark chamber received a foot shock (0.3 mA, 3 s). On day 10 (retention), step-through latency (maximum 300 s) was recorded. Animals with training latency <10 s or no shock response (sensitivity score = 0) were excluded (2 mice/119).

Statistical Analysis. Data (mean ± SEM) were analyzed by One-way ANOVA (Dunnett's post-hoc) for Y-maze and biochemical data. Kruskal-Wallis ANOVA (Dunn's post-hoc) for passive avoidance latencies Significance threshold: *p < 0.05, **$p < 0.01$, ***$p < 0.001$ (GraphPad Prism).

CRediT authorship contribution statement

Feng He: Writing – original draft, Methodology, Data curation, Conceptualization. **Julian Hofmann:** Methodology, Formal analysis, Data curation. **Eleonora Poeta:** Methodology, Formal analysis, Data curation. **Barbara Monti:** Writing – review & editing, Supervision. **Lucie Crouzier:** Methodology, Formal analysis, Data curation. **Tangui Maurice:** Writing – review & editing, Supervision. **Michael Decker:** Writing – review & editing, Supervision, Project administration, Funding acquisition, Conceptualization.

Declaration of competing interest

The authors declare that they have no known competing financial interests or personal relationships that could have appeared to influence the work reported in this paper.

Acknowledgements

M.D. acknowledges the German Research Council (Deutsche Forschungsgemeinschaft) under DFG DE 1546/6-3. M.D. and T.M. acknowledge support from Campus France (PHC Procope) and the German Academic Exchange Service (DAAD) with funds of the Federal Ministry of Education and Research (BMBF) under grant # 57387204, as well as support from **BayFrance** (Franco-Bavarian University

cooperation center) under grant # FK03-2020. F.H. acknowledges the Ph.D. scholarship from the China Scholarship Council (CSC), Science & Technology Program of Medical & Health of Zhejiang Province (2024KY1300), Zhejiang Province Traditional Chinese Medicine Science and Technology Project (2025ZR162) and Zhejiang Provincial Natural Science Foundation (LQN25H120006). T.M. and M.D. acknowledge the Agence Nationale de la Recherche and the Deutsche Forschungsgemeinschaft for a cooperative DFG/ANR grant (project ANR-22-CE92-0080 and DFG DE 1546/12-1).

Appendix A. Supplementary data

Supplementary data to this article can be found online at https://doi.org/10.1016/j.ejmech.2025.118068.

Data availability

Data will be made available on request.

References

[1] A. Paula, A.C. Rodrigo, O. Catarina, Neuroinflammation, oxidative stress and the pathogenesis of alzheimers disease, Curr. Pharm. Des. 16 (2010) 2766–2778.
[2] J. Lewerenz, G. Ates, A. Methner, M. Conrad, P. Maher, Oxytosis/ferroptosis-(re-) emerging roles for oxidative stress-dependent non-apoptotic cell death in diseases of the central nervous system, Front. Neurosci. 12 (2018) 214.
[3] F. Kametani, M. Hasegawa, Reconsideration of amyloid hypothesis and tau hypothesis in alzheimer's disease, Front. Neurosci. 12 (2018) 25.
[4] T. Shirlee, S. David, M. Pamela, Oxytosis: a novel form of programmed cell death, Curr. Top. Med. Chem. 1 (2001) 497–506.
[5] P. Maher, A. Currais, D. Schubert, Using the oxytosis/ferroptosis pathway to understand and treat age-associated neurodegenerative diseases, Cell Chem. Biol. 27 (2020) 1456–1471.
[6] S.J. Dixon, K.M. Lemberg, M.R. Lamprecht, R. Skouta, E.M. Zaitsev, C.E. Gleason, D.N. Patel, A.J. Bauer, A.M. Cantley, W.S. Yang, B. Morrison 3rd, B.R. Stockwell, Ferroptosis: an iron-dependent form of nonapoptotic cell death, Cell 149 (2012) 1060–1072.
[7] S. Schramm, G. Huang, S. Gunesch, F. Lang, J. Roa, P. Hogger, R. Sabate, P. Maher, M. Decker, Regioselective synthesis of 7-O-esters of the flavonolignan silibinin and SARs lead to compounds with overadditive neuroprotective effects, Eur. J. Med. Chem. 146 (2018) 93–107.
[8] S. Gunesch, M. Hoffmann, C. Kiermeier, W. Fischer, A.F.M. Pinto, T. Maurice, P. Maher, M. Decker, 7-O-Esters of taxifolin with pronounced and overadditive effects in neuroprotection, anti-neuroinflammation, and amelioration of short-term memory impairment in vivo, Redox Biol. 29 (2020) 101378.
[9] S. Gunesch, D. Soriano-Castell, S. Lamer, A. Schlosser, P. Maher, M. Decker, Development and application of a chemical probe based on a neuroprotective flavonoid hybrid for target identification using activity-based protein profiling, ACS Chem. Neurosci. 11 (2020) 3823–3837.
[10] M. Hoffmann, C. Stiller, E. Endres, M. Scheiner, S. Gunesch, C. Sotriffer, T. Maurice, M. Decker, Highly selective butyrylcholinesterase inhibitors with tunable duration of action by chemical modification of transferable carbamate units exhibit pronounced neuroprotective effect in an alzheimer's disease mouse model, J. Med. Chem. 62 (2019) 9116–9140.
[11] M. Scheiner, M. Hoffmann, F. He, E. Poeta, A. Chatonnet, B. Monti, T. Maurice, M. Decker, Selective pseudo-irreversible butyrylcholinesterase inhibitors transferring antioxidant moieties to the enzyme show pronounced neuroprotective efficacy in vitro and in vivo in an alzheimer's disease mouse model, J. Med. Chem. 64 (2021) 9302–9320.
[12] M. Scheiner, D. Dolles, S. Gunesch, M. Hoffmann, M. Nabissi, O. Marinelli, M. Naldi, M. Bartolini, S. Petralla, E. Poeta, B. Monti, C. Falkeis, M. Vieth, H. Hübner, P. Gmeiner, R. Maitra, T. Maurice, M. Decker, Dual-acting cholinesterase–human cannabinoid receptor 2 ligands show pronounced neuroprotection in vitro and overadditive and disease-modifying neuroprotective effects in vivo, J. Med. Chem. 62 (2019) 9078–9102.
[13] J. Hofmann, T. Ginex, A. Espargaro, M. Scheiner, S. Gunesch, M. Arago, C. Stigloher, R. Sabate, F.J. Luque, M. Decker, Azobioisosteres of curcumin with pronounced activity against amyloid aggregation, intracellular oxidative stress, and neuroinflammation, Chem. Eur J. 27 (2021) 6015–6027.
[14] B.J. Josey, E.S. Inks, X. Wen, C.J. Chou, Structure-activity relationship study of vitamin k derivatives yields highly potent neuroprotective agents, J. Med. Chem. 56 (2013) 1007–1022.
[15] A. Paul, G.K. Viswanathan, S. Mahapatra, G. Balboni, S. Pacifico, E. Gazit, D. Segal, Antagonistic activity of naphthoquinone-based hybrids toward amyloids associated with Alzheimer's disease and type-2 diabetes, ACS Chem. Neurosci. 10 (2019) 3510–3520.
[16] M. Frenkel-Pinter, S. Tal, R. Scherzer-Attali, M. Abu-Hussien, I. Alyagor, T. Eisenbaum, E. Gazit, D. Segal, Naphthoquinone-tryptophan hybrid inhibits aggregation of the tau-derived peptide PHF6 and reduces neurotoxicity, J. Alzheimers Dis. 51 (2016) 165–178.
[17] E. Mishima, J. Ito, Z. Wu, T. Nakamura, A. Wahida, S. Doll, W. Tonnus, P. Nepachalovich, E. Eggenhofer, M. Aldrovandi, B. Henkelmann, K.-i. Yamada, J. Wanninger, O. Zilka, E. Sato, R. Feederle, D. Hass, A. Maida, A.S.D. Mourão, A. Linkermann, E.K. Geissler, K. Nakagawa, T. Abe, M. Fedorova, B. Proneth, D. A. Pratt, M. Conrad, A non-canonical vitamin K cycle is a potent ferroptosis suppressor, Nature 608 (2022) 778–783.
[18] E. Nepovimova, J. Korabecny, R. Dolezal, K. Babkova, A. Ondrejicek, D. Jun, V. Sepsova, A. Horova, M. Hrabinova, O. Soukup, N. Bukum, P. Jost, L. Muckova, J. Kassa, D. Malinak, M. Andrs, K. Kuca, Tacrine–trolox hybrids: a novel class of centrally active, nonhepatotoxic multi-target-directed ligands exerting anticholinesterase and antioxidant activities with low in vivo toxicity, J. Med. Chem. 58 (2015) 8985–9003.
[19] F. He, C.J. Chou, M. Scheiner, E. Poeta, N. Yuan Chen, S. Gunesch, M. Hoffmann, C. Sotriffer, B. Monti, T. Maurice, M. Decker, Melatonin- and ferulic acid-based HDAC6 selective inhibitors exhibit pronounced immunomodulatory effects in vitro and neuroprotective effects in a pharmacological alzheimer's disease mouse model, J. Med. Chem. 64 (2021) 3794–3812.
[20] M. Scheiner, M. Hoffmann, F. He, E. Poeta, A. Chatonnet, B. Monti, T. Maurice, M. Decker, Selective pseudo-irreversible butyrylcholinesterase inhibitors transferring antioxidant moieties to the enzyme show pronounced neuroprotective efficacy in vitro and in vivo in an Alzheimer's disease mouse model, J. Med. Chem. 64 (2021) 9302–9320.
[21] M. Falsini, D. Catarzi, F. Varano, C. Ceni, D. Dal Ben, G. Marucci, M. Buccioni, R. Volpini, L. Di Cesare Mannelli, E. Lucarini, C. Ghelardini, G. Bartolucci, M. Menicatti, V. Colotta, Antioxidant-conjugated 1,2,4-triazolo[4,3-a]pyrazin-3-one derivatives: highly potent and selective human A2A adenosine receptor antagonists possessing protective efficacy in neuropathic pain, J. Med. Chem. 62 (2019) 8511–8531.
[22] A. Daina, O. Michielin, V. Zoete, SwissADME: a free web tool to evaluate pharmacokinetics, drug-likeness and medicinal chemistry friendliness of small molecules, Sci. Rep. 7 (2017) 42717.
[23] W.S. Yang, R. SriRamaratnam, M.E. Welsch, K. Shimada, R. Skouta, V. S. Viswanathan, J.H. Cheah, P.A. Clemons, A.F. Shamji, C.B. Clish, L.M. Brown, A. W. Girotti, V.W. Cornish, S.L. Schreiber, B.R. Stockwell, Regulation of ferroptotic cancer cell death by GPX4, Cell 156 (2014) 317–331.
[24] W.S. Yang, B.R. Stockwell, Synthetic lethal screening identifies compounds activating iron-dependent, nonapoptotic cell death in oncogenic-RAS-harboring cancer cells, Chem. Biol. 15 (2008) 234–245.
[25] C. Chiruta, D. Schubert, R. Dargusch, P. Maher, Chemical modification of the multitarget neuroprotective compound fisetin, J. Med. Chem. 55 (2012) 378–389.
[26] W.D. Saputra, N. Aoyama, M. Komai, H. Shirakawa, Menaquinone-4 suppresses lipopolysaccharide-induced inflammation in MG6 mouse microglia-derived cells by inhibiting the NF-kappaB signaling pathway, Int. J. Mol. Sci. 20 (2019) 2317.
[27] Y. Ohsaki, H. Shirakawa, A. Miura, P.E. Giriwono, S. Sato, A. Ohashi, M. Iribe, T. Goto, M. Komai, Vitamin K suppresses the lipopolysaccharide-induced expression of inflammatory cytokines in cultured macrophage-like cells via the inhibition of the activation of nuclear factor κB through the repression of IKKα/β phosphorylation, J. Nutr. Biochem. 21 (2010) 1120–1126.
[28] X. Li, R.A. Himes, L.C. Prosser, C.F. Christie, E. Watt, S.F. Edwards, C.S. Metcalf, P. J. West, K.S. Wilcox, S.S.L. Chan, C.J. Chou, Discovery of the first vitamin K analogue as a potential treatment of pharmacoresistant seizures, J. Med. Chem. 63 (2020) 5865–5878.
[29] T. Maurice, B.P. Lockhart, A. Privat, Amnesia induced in mice by centrally administered β-amyloid peptides involves cholinergic dysfunction, Brain Res. 706 (1996) 181–193.
[30] A. Carles, M. Hoffmann, M. Scheiner, L. Crouzier, C. Bertrand-Gaday, A. Chatonnet, M. Decker, T. Maurice, The selective butyrylcholinesterase inhibitor UW-MD-95 shows symptomatic and neuroprotective effects in a pharmacological mouse model of alzheimer's disease, CNS Neurosci, Ther. 30 (2024) e14814.
[31] N.Y. Yamada K, T. Hasegawa, Y. Komori, T. Nikai, H. Sugihara, T. Nabeshima, The role of nitric oxide in dizocilpine-induced impairment of spontaneous alternation behavior in mice, J. Pharmacol. Exp. Therapeut. 276 (1996) 460–466.
[32] O.P. Sharma, T.K. Bhat, DPPH antioxidant assay revisited, Food Chem. 113 (2009) 1202–1205.
[33] B. Ou, M. Hampsch-Woodill, R.L. Prior, Development and validation of an improved oxygen radical absorbance capacity assay using fluorescein as the fluorescent probe, J. Agric. Food Chem. 49 (2001) 4619–4626.
[34] A. Dávalos, C. Gómez-Cordovés, B. Bartolomé, Extending applicability of the oxygen radical absorbance capacity (ORAC−fluorescein) assay, J. Agric. Food Chem. 52 (2004) 48–54.